Predicting slowdowns in decadal climate warming trends with explainable neural networks

Zachary M. Labe[1,1] and Elizabeth A. Barnes[1,1]

[1]Colorado State University

November 30, 2022

Abstract

The global mean surface temperature (GMST) record exhibits both interannual to multidecadal variability and long-term warming due to external climate forcing. To explore the predictability of temporary slowdowns in decadal warming, we apply an artificial neural network (ANN) to climate model data from the Community Earth System Model Version 2 Large Ensemble Project. Here, an ANN is tasked with whether or not there will be a slowdown in the rate of the GMST trend by using maps of ocean heat content at the onset. Through a machine learning explainability method, we find the ANN is learning off-equatorial patterns of anomalous ocean heat content that resemble transitions in the phase of the Interdecadal Pacific Oscillation in order to make slowdown predictions. Finally, we test our ANN on observed historical data, which further reveals how explainable neural networks are useful tools for understanding decadal variability in both climate models and observations.

Predicting slowdowns in decadal climate warming trends with explainable neural networks

Zachary M. Labe[1] **and Elizabeth A. Barnes**[1]

[1]Department of Atmospheric Science, Colorado State University, Fort Collins, CO, USA

Key Points:

- An artificial neural network predicts the onset of slowdowns in decadal warming trends of global mean surface temperature
- Explainable AI reveals the neural network is leveraging tropical patterns of ocean heat content anomalies to make its predictions
- Transitions in the phase of the Interdecadal Pacific Oscillation are frequently associated with warming slowdown predictions in CESM2-LE

Corresponding author: Zachary M. Labe, zmlabe@rams.colostate.edu

Abstract

The global mean surface temperature (GMST) record exhibits both interannual to multidecadal variability and a long-term warming trend due to external climate forcing. To explore the predictability of temporary slowdowns in decadal warming, we apply an artificial neural network (ANN) to climate model data from the Community Earth System Model Version 2 Large Ensemble. Here, an ANN is tasked with whether or not there will be a slowdown in the rate of the GMST trend by using maps of ocean heat content at the onset. Through a machine learning explainability method, we find the ANN is learning off-equatorial patterns of anomalous ocean heat content that resemble transitions in the phase of the Interdecadal Pacific Oscillation in order to make slowdown predictions. Finally, we test our ANN on observed historical data, which further reveals how explainable neural networks are useful tools for understanding decadal variability in both climate models and observations.

Plain Language Summary

Long-term observations reveal that Earth's average temperature is rising due to human-caused climate change. Along with this warming trend are also variations from year-to-year and even over multiple decades. This temperature variability is often tied to regional patterns of heat in the deep ocean, which can then modulate weather and climate extremes over land. In an attempt to better predict temperature variability on decadal timescales, we use a machine learning method called artificial neural networks and data from a climate model experiment, which was designed to compare climate change and variability. Here, our artificial neural network uses maps of ocean heat to predict the onset of temporary slowdowns in the rate of global warming in both the climate model and in real-world observations. We then use a visualization technique to find which areas of ocean heat that the artificial neural network is using to make its correct predictions, which are found to be mainly across the Pacific Ocean. In agreement with recent research, our study finds that new data science methods, like machine learning, can be useful tools for predicting variations in global climate.

1 Introduction

One of the most recognizable indicators of anthropogenic climate change is the positive trend in global mean surface temperature (GMST) (Hansen et al., 2010; Johnson

et al., 2020). GMST also exhibits interannual to multidecadal variability with periods of accelerations and slowdowns in the rate of decadal trends (Trenberth et al., 2002; Thompson et al., 2009; Dai et al., 2015; Maher et al., 2020). A notable example of one of these GMST slowdowns occurred in the early 2000s (Flato et al., 2013; Fyfe et al., 2013). This temporary warming slowdown ended in the mid-2010s (Mann et al., 2017; Zhang et al., 2019), and more recently, 2020 was one of the three warmest years in the observational record (Dunn et al., 2021). Although the early 2000s was commonly described as a 'hiatus' or 'pause' in global warming within scientific studies and popular media (Boykoff, 2014; Lewandowsky et al., 2016), we will refer to it here as a 'slowdown in decadal warming' (Fyfe et al., 2016), which is more consistent with our understanding of internal variability in the climate system.

Numerous mechanisms have been proposed to explain the cause of the early 2000s slowdown, as reviewed in Medhaug et al. (2017) and Xie and Kosaka (2017), but it was likely a combination of factors ranging from uncertainties in the observational data record (e.g., Cowtan & Way, 2014; Karl et al., 2015), fluctuations in radiative forcing (Schmidt et al., 2014), cooling in the eastern Pacific associated with a negative phase of the Interdecadal Pacific Oscillation (IPO) (Meehl, Hu, et al., 2013; England et al., 2014; Roberts et al., 2015), anthropogenic aerosol and volcanic forcing (Santer et al., 2014; Smith et al., 2016), changes in deep ocean heat uptake (Watanabe et al., 2013), top-of-atmosphere (TOA) energy imbalance (Meehl et al., 2011; Hedemann et al., 2017), and interactions between other modes of climate variability (W. Liu & Xie, 2018). Motivated by the increasing body of literature on the causes and impacts of the early 2000s slowdown, we aim to investigate the predictability of similar temporary GMST slowdowns occurring in a warming climate. While decadal predictability has been explored using other statistical methods (e.g., Mann et al., 2016; Sévellec & Drijfhout, 2018), sensitivity experiments (e.g. Kosaka & Xie, 2013), and hindcasts with initialized state climate modeling frameworks (e.g., Fyfe et al., 2011; Guemas et al., 2013; Meehl et al., 2014; Meehl & Teng, 2014; Boer et al., 2016), we explore this problem through the lens of machine learning.

Deep learning methods, such as neural networks, have the ability to extract and leverage nonlinear patterns across data-intensive spatial fields, which make them promising tools for revealing new insights and sources of predictability in climate science (Reichstein et al., 2019; Barnes, Mayer, et al., 2020; Irrgang et al., 2021; Sonnewald et al., 2021). Re-

cent work has demonstrated the utility for neural networks in identifying climate modes, teleconnections, and forecasts of opportunity for a wide variety of timescales (e.g., Wu & Hsieh, 2004; Ham et al., 2019; Toms et al., 2021; Gibson et al., 2021; Gordon et al., 2021; J. Liu et al., 2021; Mayer & Barnes, 2021; Nadiga, 2021; Tang & Duan, 2021). Further, a growing number of explainable artificial intelligence (XAI) methods have been adapted for applications in weather and climate science (McGovern et al., 2019; Toms et al., 2020), which can retrospectively trace the decisions of neural networks and compare the attribution of input features to known physical mechanisms in the Earth system. Besides evaluating trust and credibility to the machine learning prediction, XAI methods can also be used for physics-guided scientific discovery and hypothesis testing (Ebert-Uphoff & Hilburn, 2020; Toms et al., 2020; Sonnewald & Lguensat, 2021).

In this study, we use an artificial neural network (ANN) to explore the predictability of decadal warming slowdowns due to variability in the upper ocean within a new large ensemble experiment and real-world observations. In addition to their predictability, we also use a complimentary XAI method to investigate the oceanic patterns that may provide insight to these temporary warming slowdowns.

2 Data and Methods

2.1 Climate Model Large Ensemble

For climate model data, we use a large ensemble experiment conducted by the Community Earth System Model Version 2 (CESM2; Danabasoglu et al., 2020) (see Supporting Information for more details). Specifically, we use simulations from the CESM2 Large Ensemble Community Project (CESM2-LE; Rodgers et al., 2021), which includes 100 ensemble members branched from the fully-coupled CESM2 preindustrial control (1850 radiative forcing conditions) using different atmospheric and oceanic initial states. CESM2-LE members follow historical Coupled Model Intercomparison Project Phase 6 (CMIP6) forcing from 1850 to 2014 and thereafter follow the SSP3-7.0 future radiative forcing (high emissions scenario) until 2100 (Eyring et al., 2016; O'Neill et al., 2016). We consider the first 50 ensemble members (1-50), which are prescribed with biomass burning emissions following CMIP6 protocol (Van Marle et al., 2017). In contrast, the second set of 50 ensemble members follow temporally smoothed biomass burning fluxes (51-100). As discussed in Rodgers et al. (2021) and Fasullo et al. (2022), this difference in biomass burn-

ing forcing has been shown to affect large-scale climate features, including the GMST record in present day.

Due to limited data availability at the time of our analysis, we analyze only 40 ensemble members within the first subset of CESM2-LE (1-50). From these 40 members, we use monthly outputs of near-surface air temperature (T2M) and sea surface temperature (SST). We also utilize monthly ocean heat content (OHC), which is derived as the vertical heat content integral between three distinct depth layers (0–100 m, OHC100; 0–300 m, OHC300; 0–700 m, OHC700); although we focus on maps of OHC100 for the actual training of our ANN. We then apply a bilinear interpolation to all variables so that they share a common (slightly coarser) latitude by longitude grid (1.9° x 2.5°). We calculate annual means from the monthly data and use the period from 1990 to 2099 to classify slowdowns in decadal warming. To focus on warming slowdowns driven by internal variability, we remove the 40-member ensemble mean from each individual ensemble in every year and grid box for SST and OHC (Phillips et al., 2020; Maher et al., 2021).

2.2 Observations

To evaluate our ANN trained on CESM2-LE for predicting the early 2000s warming slowdown in the historical record, we use SST and T2M from the European Centre for Medium-Range Weather Forecasts (ECMWF) ERA5 reanalysis (Hersbach et al., 2020) and OHC from the Institute of Atmospheric Physics (IAP) ocean gridded product (Cheng & Zhu, 2016; Cheng et al., 2017) (both data sets referred to here as "observations"). SSTs from ERA5 are an interpolated product between HadISST2 (Titchner & Rayner, 2014) from January 1979 to August 2007 and OSTIA (Donlon et al., 2012) from September 2007 to present. Overall, both regional and global mean time series of SST and T2M are consistent with other observational data sets (Hersbach et al., 2020; Bell et al., 2021), including decadal trends (Figure S1). Gridded upper OHC from IAP also compares well with in situ measurements and is based on temperature data from the World Ocean Database (WOD; Boyer et al., 2013), which is then further bias-corrected, interpolated, and quality controlled (Li-Jing et al., 2015; Cheng et al., 2017).

In all observations, we use monthly output and bilinearly interpolate these fields onto the same 1.9° x 2.5° grid as CESM2-LE before calculating annual means. We linearly detrend each grid point (over 1979 to 2020) for SST and OHC predictors to remove

long-term warming signals and thus focus on patterns of interannual variability for slowdown predictions.

2.3 Defining Slowdowns in Decadal Warming

Figure 1 shows an example of how we define warming slowdown events in CESM2-LE and observations. While there have been numerous definitions and data sets used for identifying warming slowdown (or so-called hiatus/pause) events (e.g., Risbey et al., 2018; Wei et al., 2021), they are often classified as a near-zero or negative 10-20 year linear trend of the GMST. Recent studies show that the frequency of slowdown events in CMIP5 models decreases substantially by the end of the 21st century using a negative 10-year linear trend definition (e.g., Maher et al., 2014; Li & Baker, 2016; Sévellec et al., 2016). Their frequency could also decrease due to increasing climate sensitivity (Modak & Mauritsen, 2021). Yet, internal variability is still projected to affect regional and global climate trends even under higher future emission scenarios (Easterling & Wehner, 2009; Li & Baker, 2016; Cassou et al., 2018; Maher et al., 2020). Here, we take a GMST slowdown threshold using decadal trends (e.g., Meehl et al., 2011; Maher et al., 2014), which is on the shorter end of previously used timescales and focus on the influence of oceanic internal variability.

First, to classify slowdown events in observations, we compute the area-weighted GMST and calculate 10-year moving linear trends beginning in 1990. We start our analysis in 1990 to avoid any multidecadal slowdown events earlier in the 20th century when the influence of the forced climate change signal may not have fully emerged (Delworth & Knutson, 2000; Papalexiou et al., 2020; Hawkins et al., 2020). We then calculate the mean of all 10-year trends between 1990 and 2020 and take one standard deviation below this mean as our threshold for slowdown events in observations (equating to about $+0.01°C/yr$, or 0.44 of the overall mean trend) (black dashed line in Figure 1b). We identify four consecutive slowdown events in observations, which begin in 2002. These years are consistent with previous studies (Lewandowsky et al., 2018) and are similarly classified in other datasets with our definition (Figure S1).

For CESM2-LE, we first compute the area-weighted GMST for the ensemble mean from all 40 members through 2099 (Figure 1a). We then calculate 10-year moving linear trends, which begin in 1990 for consistency with observations. The climate model

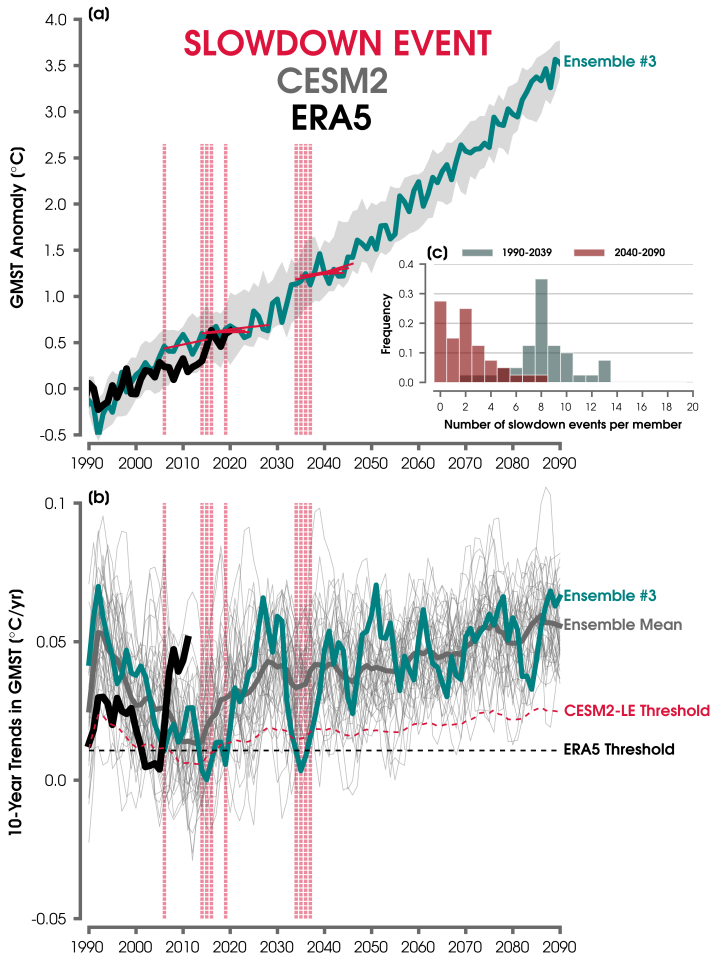

Figure 1. (a) Time series showing annual-mean GMST anomalies for one example (ensemble member) in CESM2-LE relative to a 1981-2010 baseline (blue line). The ensemble spread in annual-mean GMST anomalies is also shown in gray shading for CESM2-LE. Annual-mean GMST anomalies from ERA5 reanalysis are indicated with a black line relative to a 1981-2010 baseline. Onset of slowdown events in the example ensemble are highlighted with red dashed (vertical) lines and their associated linear trends (red lines) over each 10-year period. (b) The slope of all 10-year moving linear trends are shown for the example ensemble member compared to the other ensembles (light gray lines) and the ensemble mean (dark gray line). As in (a), red dashed (vertical) lines are shown for the onset of slowdown events in the highlighted ensemble member. Slopes of all 10-year moving linear trends are shown for ERA5 reanalysis by the black solid line. The threshold for slowdown events in CESM2-LE is shown with a red dashed line, and the threshold for slowdown events in ERA5 is shown with a black dashed line. (c) Histogram showing the frequency of slowdown events in each ensemble member over the 1990-2039 period (gray bars) and the 2040-2090 period (red bars). See Section 2.3 for more details.

threshold for a slowdown (red dashed line in Figure 1b) is defined by multiplying the fraction of the mean trend from the observations (0.44) times each of the ensemble mean decadal trends (thick gray line in Figure 1b).

Separately, we also calculate the GMST for each ensemble member and the associated moving 10-year linear trends (thin gray lines in Figure 1b). We define a warming slowdown event when these 10-year trends fall below the climate model threshold. That is, we define a slowdown event as a fraction of the forced response. However, our definition still leads to a reduction in the number of slowdown events after 2040 in CESM2-LE (Figure 1c), as shown in several past studies (e.g., Sévellec et al., 2016).

2.4 Artificial Neural Network

For this analysis, we adopt a neural network architecture that is designed to receive input maps of OHC100 and output whether the next 10 years will observe a decadal warming slowdown. In other words, if we input a map of OHC100 for the year 2000, the ANN will output whether the decade from 2000 to 2009 will be a slowdown event or not. A schematic of our ANN can be found in Figure S3, and the architecture parameters are outlined in the Supporting Information.

In addition to seeing if warming slowdown events are predictable, we are also interested in the sources of predictability in fields of anomalous OHC100. To attempt to understand the ANN's decision-making process, we use a method of XAI called layer-wise relevance propagation (LRP; Bach et al., 2015; Montavon et al., 2017, 2018). The utility of LRP has been demonstrated in a wide range of weather and climate applications (e.g., Barnes, Toms, et al., 2020; Davenport & Diffenbaugh, 2021; Gordon et al., 2021; Labe & Barnes, 2021; Sonnewald & Lguensat, 2021), and an overview for the geosciences can be found in Toms et al. (2020). In short, prior to the softmax, a single prediction output is propagated backward through the ANN after freezing the model weights and biases. LRP then returns a vectorized spatial map, which shows the feature relevance for every input sample's latitude and longitude pixel. Therefore, we have a unique LRP heatmap for every input sample of OHC100. Throughout this study, regions of higher relevance can be interpreted as more important for the ANN's prediction. We implement the LRP_z rule for back propagation, which was found by Mamalakis et al. (2021) to be a well performing XAI method using a benchmark climate data set similar to ours. To

improve interpretation and reduce the amount of noise in the LRP heatmaps, we only focus on positive areas of relevance, which are features that contribute positively to the ANN's prediction output.

3 Results

3.1 Predicting Slowdown Trends in a Large Ensemble

Figure 2a shows the results of our ANN for each CESM2-LE ensemble member in the testing data set from 1990 through 2090 (i.e., 2090-2099 is the last complete decade of data). Given the large class imbalance, we focus on the F1 score (balancing precision and recall), rather than categorical accuracy, to evaluate the performance of our ANN for correctly identifying slowdown events. Figure S7 provides a collection of skill metrics for our testing data. Overall, the network achieves a F1 score of 40% and performs better than random chance (10.4%). While our ANN sometimes struggles with correctly classifying slowdown events, especially those that occur simultaneously in a row, it generally classifies at least one 10 year period during these extended events. This skill suggests that the ANN is learning information from OHC100 that corresponds to future slowdown periods in CESM2-LE.

We test the robustness of our results by training 100 ANNs with unique random initialization seeds and different combinations of ensemble members used for training, validation, and testing data. The F1 score of our single seed ANN falls within the $\approx$ 85th percentile of this distribution, and additional metric scores are shown in Figure S8 for the 100 ANNs. The spread between this distribution can be attributed to uncertainties from random initialization states of the ANNs and different combinations of ensemble members. Although we found that there is no relationship between the accuracy of testing predications compared to the number of training slowdown events each ANN learned for the 100 iterations (Figure S9).

3.2 Sources of Predictability for Slowdowns

To understand the sources of skill for the ANN's correct slowdown predictions in CESM2-LE, we turn to composite maps of LRP. Recall that LRP traces the decision-making process of a neural network, where higher relevance corresponds to greater importance for the ANN to make its final prediction. While we have LRP heatmaps for ev-

ery input of annual-mean OHC100, we focus on correct predictions by the ANN in the testing data set. Figure 2b shows the LRP composite for all correct slowdown predictions. We find higher relevance in the off-equatorial regions of the eastern Pacific, especially in the regions of the North/South Pacific Meridional Modes (Amaya, 2019). There are also patches of higher relevance across portions of the Indian Ocean, south Atlantic, and south Pacific, which suggests that the ANN is leveraging other regional patterns of OHC to make predictions. Notably, there is no relevance for a thin band along the equator in the area of the El Niño-Southern Oscillation (ENSO). Figure 2d shows the corresponding LRP composite for no slowdowns in decadal warming, which is nearly a mirror image of Figure 2b. This is a product of the setup of our binary classification problem, and therefore the LRP maps reveal the regions that the ANN is using to make this determination (i.e., yes or no slowdown).

We compare these LRP maps to composites of the raw (normalized) OHC data that were input to the network for correct slowdown predictions (Figure 2c) versus correct no slowdown predictions (Figure 2e). Now we find striking differences between the two OHC patterns. The composite of OHC100 for the slowdown predictions reveal an IPO-like spatial pattern with cold pools in the west-central North Pacific and west-central South Pacific and warm anomalies in the Southern Ocean and eastern Pacific. We also see the signature of a positive Indian Ocean Dipole (IOD; Saji et al., 1999) and a dipole pattern of OHC100 anomalies between the southern Atlantic and north-central Atlantic. Some studies have shown that a positive IOD can be a precursor for a rapid transition to a cooler equatorial Pacific by modulating the strength of the Walker Circulation (Izumo et al., 2010; Le et al., 2020; Yoo et al., 2020).

Figure S10 shows maps of OHC at other vertical depth levels for the slowdown predictions compared to 5-10 years after the start of the slowdown decade. We find a similar spatial pattern of SSTs (Figure S10a), but a stronger cold pool at deeper depths, which appears to be propagating eastward in the equatorial Pacific (Figure S10c-d). In contrast, we find a negative IPO-like pattern for the composites at the end of the slowdown decade (Figure S10e-h). This finding is in agreement with earlier studies that showed slowdowns in decadal warming often correspond to trends toward a negative phase of the IPO within CMIP5 models (e.g., Maher et al., 2014). Given this evolution of events and the patterns of LRP relevance, it is feasible that the ANN is learning OHC anomalies associated with transitions in the state of the IPO.

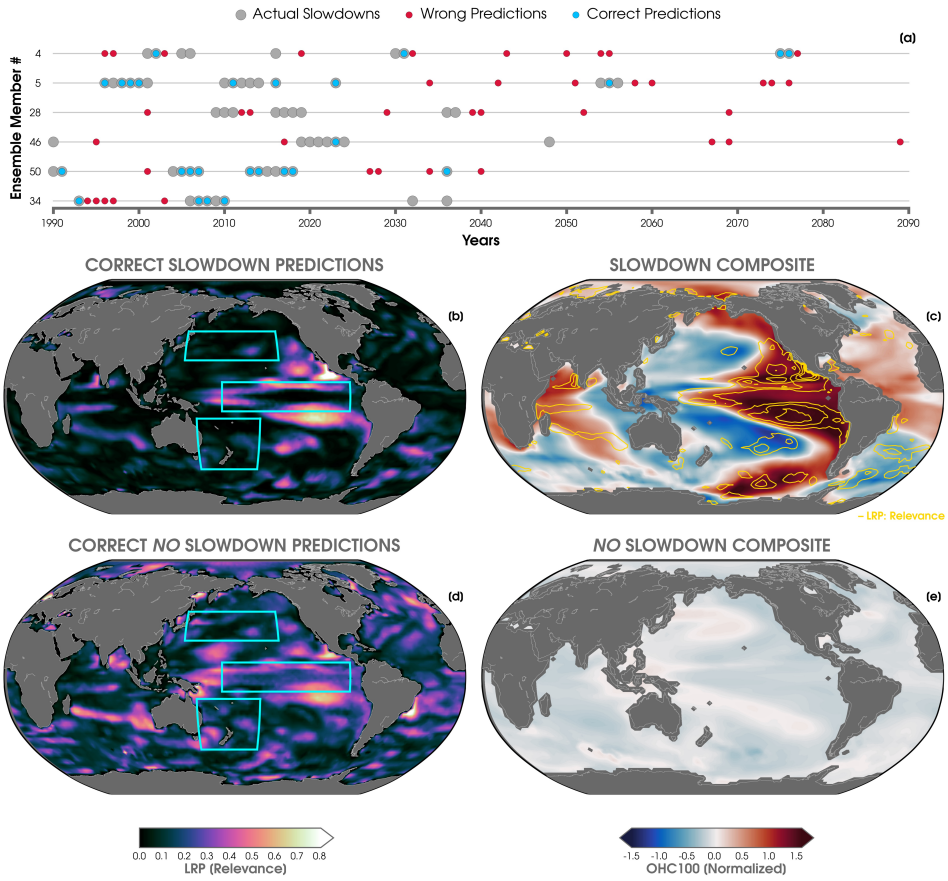

Figure 2. (a) Time series showing the results in each ensemble member of the testing data for the onset of actual slowdown events (gray dots), incorrect slowdown predictions by the ANN (red dots), and correct slowdown predictions by the ANN (blue dots). (b) LRP composite heatmap for the correct slowdown predictions by the ANN (testing data). Higher LRP values indicate greater relevance for the ANN's prediction. LRP values are normalized by the maximum relevance in the composite for visualization purposes. Blue boxes highlight regions of the Tripole Index for the IPO (Henley et al. (2015); 25°N-45°N and 140°E-145°W, 10°S-10°N and 170°E-90°W, 50°S-15°S and 150°E-160°W). (c) Composite of normalized OHC100 for correct slowdown predictions. Yellow contour lines are overlaid to show relevance from the LRP composite in (b). (d) As in (b), but for correct predictions of no slowdowns in decadal warming. (e) As in (c), but for correct predictions of no slowdowns in decadal warming.

To directly assess the IPO in the maps of OHC100, we compute the unfiltered IPO Tripole Index (normalized) following Henley et al. (2015) using annual-mean SSTs from CESM2-LE (Figure S11). As expected from the composite analysis in Figure 2, we find that correct predictions of slowdowns generally correspond to highly positive phases of the IPO index. To demonstrate this point, we select one ensemble member and compare its annual IPO index to the frequency of the slowdowns classifications in the distribution of 100 unique ANNs (Figure S12). We find slowdown predictions often correspond to a positive IPO index in this ensemble member, but also importantly, not every positive IPO results in the prediction of a slowdown event.

To further confirm that the ANN is learning additional spatial information than simply a reflection of the IPO-like pattern of OHC anomalies, we set up a logistic regression problem by inputting only the value of the IPO index in CESM2-LE to predict whether a slowdown event will occur over the next 10 years (F1 score = 0.28). Thus, we find that using global maps of OHC100 as inputs to the fully-connected ANN provides more skillful predictions of warming slowdown events.

3.3 Predicting Slowdown Trends in Observations

Lastly, we test the utility of our neural network for capturing the observed early 2000s slowdown by inputting maps of OHC100 from observations, which are first linearly detrended and then normalized by their own mean and standard deviation at every grid point. Figure 3a shows the slowdown prediction from our ANN for each input map of annual-mean OHC100 using observations. During the overlapping period with the actual early 2000s slowdown, the decades from 2003 to 2012 and 2004 to 2013 are classified as warming slowdowns. The range in observational predictions across the distribution of 100 ANNs is also shown in Figure S13.

To understand the patterns of anomalous OHC100 that the ANN is using to make a prediction in observations, we evaluate a LRP composite map from the single seed ANN (which correctly predicted two slowdown events in the early 2000s) in Figure S14a. Similar to the LRP composites using CESM2-LE (Figure 2), we find areas of higher relevance in the equatorial western Pacific, south-central Atlantic, and patches in the Indian Ocean. The ANN also predicts the onset of slowdown events mainly during positive phases of the IPO (Figure 3b). Although this correlation is not always the case (e.g., during the

Figure 3. (a)Time series showing the slowdown onset predictions by the ANN (dashed red line). Green bars show the onset of actual slowdown events in observations. Gray shading indicates 10-year trend periods that extend into the future (e.g., 2012-2021). (b) Time series of the unfiltered Tripole IPO Index (normalized) for each year in observations (red/blue bars). Green bars show the onset of actual slowdown events in observations.

positive IPO event in the early 1990s), which again suggests that our ANN is leveraging additional spatial information than simply the IPO pattern to make predictions. This is also supported by our interpretation of the LRP maps, which show higher relevance regions across the western Pacific and not necessarily the canonical IPO/PDO patterns (Parker et al., 2007; Newman et al., 2016) (Figure S14a).

At the time of our analysis, the last complete decade of GMST observations covers the decade of 2011 to 2020 (Figure 1a). However, since we only need OHC prior to predicting the future 10 years, we can also explore warming slowdown events extending beyond 2020 (Figure 3a). For these future predictions, 2016 to 2025 and 2017 to 2026

are classified as warming slowdown events by the ANN. 2016 was characterized by the dissipation of an extreme El Niño event into a weak La Niña state (Santoso et al., 2017), and the GMST also set a new record high for that respective year (Aaron-Morrison et al., 2017). Similarly, the IPO index also shows a transition from a highly positive phase in 2015 to a neutral or negative phase in the following years through 2020 (Figure 3b). Composites of normalized SST and OHC for 2016 and 2017 show anomalously warm subsurface waters just off the equator in the eastern Pacific and cold pools in the tropical Indo-Pacific and north-central Pacific (Figure S15). Comparing the LRP composite map over 2016 and 2017 with the raw OHC100 anomalies (Figure S14b and Figure S15b), we find higher relevance outlining the warm anomalies in the eastern Pacific and patches of relevance in the Indian Ocean and southern Pacific. The LRP composite for the future slowdown prediction in Figure S14b is more similar to those outlined in CESM2-LE (e.g., Figure 2b), which may provide insight for why the ANN more confidently predicts a slowdown compared to the earlier 2000s event.

4 Summary and Conclusions

Due to an increasing need from decision makers and other community stakeholders for near-term climate predictions, there has been a coordinated effort to increase the availability of decadal outlooks from initialized climate models and other operational forecast systems (e.g. Graham et al., 2011; Meehl, Goddard, et al., 2013; Boer et al., 2016; Smith et al., 2019; Kushnir et al., 2019; Merryfield et al., 2020; Hewitt et al., 2021; Meehl et al., 2021). However, these simulations can be computationally expensive to run. Alternatively, recent progress in machine learning has shown promising results for decadal climate applications, especially when combined with explainability methods (e.g., Gordon et al., 2021; G. Liu et al., 2021; Toms et al., 2021). Motivated by this new line of research, we explore the utility of a relatively shallow ANN for predicting temporary decadal warming slowdowns of GMST using upper OHC variability. Although our ANN is trained on climate model data from CESM2-LE, we find that it also produces skillful predictions of the early 2000s warming slowdown in observational data. We further compliment our ANN with a machine learning explainability method (LRP) to attempt to understand what information the ANN is using to make its correct predictions. The LRP maps reveal that the ANN is mainly using off-equatorial anomalies of OHC100 to predict the onset of a decadal warming slowdown. These patterns suggest that the ANN may be learn-

ing precursors for transitions to a negative phase of the IPO, although this topic remains an active area of research (Cai et al., 2019; Power et al., 2021).

Finally, we note a few important considerations when interpreting these results. First, the causal mechanisms related to the early 2000s slowdown event remain uncertain (Hedemann et al., 2017; von Känel et al., 2017; Medhaug et al., 2017), and we note that we have only considered one potential predictor for warming slowdowns (i.e., upper OHC). Slowdowns can also occur due to external forcing (e.g., aerosols) or other modes of climate variability (Medhaug et al., 2017). Further, there are a number of different definitions for slowdown-like events (Risbey et al., 2018). Future work could explore the predictability of slowdowns using ANNs with other climate predictors, such as considering a TOA energy imbalance approach (Hedemann et al., 2017), or taking into account longer duration events. It may also be valuable to combine maps of OHC at different lead times, which was recently demonstrated by Gordon et al. (2021) for predicting transitions in the phase of the PDO. Lastly, we train our ANN on a large ensemble from only one climate model. Thus, our results may be influenced CESM2's inherent model biases and prescribed external forcing, including the SSP3-7.0 emissions scenario and the protocol for biomass burning (Rodgers et al., 2021). The value of adding more complexity to the ANN and using multi-model large ensembles will be left for future exploration. Importantly, even our simple ANN demonstrates that temporary warming slowdowns may have some predictability from Pacific climate variability and demonstrates a new application of machine learning for climate science.

Open Research

Climate model data used in this study are freely available from the CESM2 Large Ensemble Project (`https://www.cesm.ucar.edu/projects/community-projects/LENS2/data-sets.html`). Computer code for the ANN architecture and exploratory data analysis is available at `https://zenodo.org/record/5879059`. Observations used in this study are from Institute of Atmospheric Physics (IAP) ocean heat content (`http://www.ocean.iap.ac.cn/`), and monthly atmospheric reanalysis data are also freely available from ERA5 (`https://cds.climate.copernicus.eu/cdsapp#!/dataset/reanalysis-era5-single-levels-monthly-means?tab=overview`), BEST (`http://berkeleyearth.org/data/`), GISTEMPv4 (`https://data.giss.nasa.gov/gistemp/`), HadCRUTv5 (`https://www.metoffice.gov.uk/hadobs/hadcrut5/data/current/download.html`),

and NCEP2 (`https://psl.noaa.gov/data/gridded/data.ncep.reanalysis.derived.surfaceflux.html`)

Conflict of Interest

The Authors declare no conflicts of interest relevant to this study.

Acknowledgments

We thank two anonymous reviewers for their constructive suggestions to improve this study. We also thank Dr. John Fasullo (NCAR) for providing fields of OHC from the CESM2 Large Ensemble and Emily M. Gordon (CSU) for other helpful discussions. This work was supported by NOAA MAPP grant NA19OAR4310289 and by the Regional and Global Model Analysis program area of the U.S. Department of Energy's Office of Biological and Environmental Research as part of the Program for Climate Model Diagnosis and Intercomparison project. We also would like to acknowledge the CESM2 Large Ensemble Community Project, supercomputing resources provided by the IBS Center for Climate Physics in South Korea, and the Cheyenne supercomputer which is operated by the Computational and Information Systems Laboratory (CISL) at NCAR (doi:105065/D5RX99HX) and supported by the National Science Foundation (NSF).

References

Aaron-Morrison, A. P., Ackerman, S. A., Adams, N. G., Adler, R. F., Albanil, A., Alfaro, E. J., ... Romanovsky, V. E. (2017, aug). State of the Climate in 2016. *Bulletin of the American Meteorological Society*, *98*(8), Si–S280. Retrieved from `https://journals.ametsoc.org/view/journals/bams/98/8/2017bamsstateoftheclimate.1.xml` doi: 10.1175/2017BAMSSTATEOFTHECLIMATE.1

Amaya, D. J. (2019, sep). The Pacific Meridional Mode and ENSO: a Review. *Current Climate Change Reports*, *5*(4), 296–307. Retrieved from `https://link.springer.com/article/10.1007/s40641-019-00142-x` doi: 10.1007/S40641-019-00142-X

Bach, S., Binder, A., Montavon, G., Klauschen, F., Müller, K. R., & Samek, W. (2015, jul). On pixel-wise explanations for non-linear classifier decisions by layer-wise relevance propagation. *PLoS ONE*, *10*(7), e0130140. Retrieved from

http://www.hfsp.org/, doi: 10.1371/journal.pone.0130140

Barnes, E. A., Mayer, K., Toms, B., Martin, Z., & Gordon, E. (2020, dec). Identifying Opportunities for Skillful Weather Prediction with Interpretable Neural Networks. *arXiv*. Retrieved from http://arxiv.org/abs/2012.07830

Barnes, E. A., Toms, B., Hurrell, J. W., Ebert-Uphoff, I., Anderson, C., & Anderson, D. (2020, sep). Indicator Patterns of Forced Change Learned by an Artificial Neural Network. *Journal of Advances in Modeling Earth Systems*, *12*(9). Retrieved from https://onlinelibrary.wiley.com/doi/10.1029/2020MS002195 doi: 10.1029/2020MS002195

Bell, B., Hersbach, H., Simmons, A., Berrisford, P., Dahlgren, P., Horányi, A., ... Thépaut, J.-N. (2021). The ERA5 Global Reanalysis: Preliminary Extension to 1950. *Quarterly Journal of the Royal Meteorological Society*. Retrieved from https://rmets.onlinelibrary.wiley.com/doi/10.1002/qj.4174 doi: 10.1002/QJ.4174

Boer, G. J., Smith, D. M., Cassou, C., Doblas-Reyes, F., Danabasoglu, G., Kirtman, B., ... Eade, R. (2016, oct). The Decadal Climate Prediction Project (DCPP) contribution to CMIP6. *Geoscientific Model Development*, *9*(10), 3751–3777. doi: 10.5194/GMD-9-3751-2016

Boyer, T., Antonov, J., Baranova, O., Coleman, C., Garcia, H., Grodsky, A., ... Zweng, M. (2013). World Ocean Database 2013. *NOAA Atlas NESDIS 72*, *NOAA Atlas*.

Boykoff, M. T. (2014, feb). Media discourse on the climate slowdown. *Nature Climate Change*, *4*(3), 156–158. Retrieved from https://www.nature.com/articles/nclimate2156 doi: 10.1038/nclimate2156

Cai, W., Wu, L., Lengaigne, M., Li, T., McGregor, S., Kug, J. S., ... Chang, P. (2019, mar). Pantropical climate interactions. *Science*, *363*(6430). Retrieved from https://www.science.org/doi/abs/10.1126/science.aav4236 doi: 10.1126/SCIENCE.AAV4236/ASSET/D6EE1BDF-355B-4FAF-9816-980B943B28E6/ASSETS/GRAPHIC/363_AAV4236_F5.JPEG

Cassou, C., Kushnir, Y., Hawkins, E., Pirani, A., Kucharski, F., Kang, I.-S., & Caltabiano, N. (2018, mar). Decadal Climate Variability and Predictability: Challenges and Opportunities. *Bulletin of the American Meteorological Society*, *99*(3), 479–490. Retrieved from https://journals

.ametsoc.org/view/journals/bams/99/3/bams-d-16-0286.1.xml doi: 10.1175/BAMS-D-16-0286.1

Cheng, L., Trenberth, K. E., Fasullo, J., Boyer, T., Abraham, J., & Zhu, J. (2017, mar). Improved estimates of ocean heat content from 1960 to 2015. *Science Advances*, *3*(3). Retrieved from https://www.science.org/doi/abs/10.1126/sciadv.1601545 doi: 10.1126/SCIADV.1601545

Cheng, L., & Zhu, J. (2016). Benefits of CMIP5 multimodel ensemble in reconstructing historical ocean subsurface temperature variations. *Journal of Climate*, *29*(15). doi: 10.1175/JCLI-D-15-0730.1

Cowtan, K., & Way, R. G. (2014, jul). Coverage bias in the HadCRUT4 temperature series and its impact on recent temperature trends. *Quarterly Journal of the Royal Meteorological Society*, *140*(683), 1935–1944. Retrieved from https://rmets.onlinelibrary.wiley.com/doi/10.1002/qj.2297 doi: 10.1002/QJ.2297

Dai, A., Fyfe, J. C., Xie, S.-P., & Dai, X. (2015, apr). Decadal modulation of global surface temperature by internal climate variability. *Nature Climate Change*, *5*(6), 555–559. Retrieved from https://www.nature.com/articles/nclimate2605 doi: 10.1038/nclimate2605

Danabasoglu, G., Lamarque, J.-F., Bacmeister, J., Bailey, D. A., DuVivier, A. K., Edwards, J., ... Strand, W. G. (2020, feb). The Community Earth System Model Version 2 (CESM2). *Journal of Advances in Modeling Earth Systems*, *12*(2), e2019MS001916. Retrieved from https://agupubs.onlinelibrary.wiley.com/doi/10.1029/2019MS001916 doi: 10.1029/2019MS001916

Davenport, F. V., & Diffenbaugh, N. S. (2021, aug). Using Machine Learning to Analyze Physical Causes of Climate Change: A Case Study of U.S. Midwest Extreme Precipitation. *Geophysical Research Letters*, *48*(15), e2021GL093787. Retrieved from https://agupubs.onlinelibrary.wiley.com/doi/10.1029/2021GL093787 doi: 10.1029/2021GL093787

Delworth, T. L., & Knutson, T. R. (2000, mar). Simulation of Early 20th Century Global Warming. *Science*, *287*(5461), 2246–2250. Retrieved from https://www.science.org/doi/abs/10.1126/science.287.5461.2246 doi: 10.1126/SCIENCE.287.5461.2246

Donlon, C. J., Martin, M., Stark, J., Roberts-Jones, J., Fiedler, E., & Wimmer, W. (2012, jan). The Operational Sea Surface Temperature and Sea Ice Analysis (OSTIA) system. *Remote Sensing of Environment*, *116*, 140–158. doi: 10.1016/J.RSE.2010.10.017

Dunn, R. J. H., Aldred, F., Gobron, N., Miller, J. B., Willett, K. M., Ades, M., ... Zotta, R. M. (2021, aug). Global Climate [in "State of the Climate in 2020"]. *Bulletin of the American Meteorological Society*, *102*(8), S11–S142. Retrieved from `https://journals.ametsoc.org/view/journals/bams/102/8/BAMS-D-21-0098.1.xml` doi: 10.1175/BAMS-D-21-0098.1

Easterling, D. R., & Wehner, M. F. (2009, apr). Is the climate warming or cooling? *Geophysical Research Letters*, *36*(8), 8706. Retrieved from `https://agupubs.onlinelibrary.wiley.com/doi/10.1029/2009GL037810` doi: 10.1029/2009GL037810

Ebert-Uphoff, I., & Hilburn, K. (2020, dec). Evaluation, Tuning, and Interpretation of Neural Networks for Working with Images in Meteorological Applications. *Bulletin of the American Meteorological Society*, *101*(12), E2149–E2170. Retrieved from `https://journals.ametsoc.org/view/journals/bams/101/12/BAMS-D-20-0097.1.xml` doi: 10.1175/BAMS-D-20-0097.1

England, M. H., McGregor, S., Spence, P., Meehl, G. A., Timmermann, A., Cai, W., ... Santoso, A. (2014, feb). Recent intensification of wind-driven circulation in the Pacific and the ongoing warming hiatus. *Nature Climate Change*, *4*(3), 222–227. Retrieved from `https://www.nature.com/articles/nclimate2106` doi: 10.1038/nclimate2106

Eyring, V., Bony, S., Meehl, G. A., Senior, C. A., Stevens, B., Stouffer, R. J., & Taylor, K. E. (2016, may). Overview of the Coupled Model Intercomparison Project Phase 6 (CMIP6) experimental design and organization. *Geoscientific Model Development*, *9*(5), 1937–1958. doi: 10.5194/gmd-9-1937-2016

Fasullo, J. T., Lamarque, J.-F., Hannay, C., Rosenbloom, N., Tilmes, S., DeRepentigny, P., ... Deser, C. (2022, jan). Spurious Late Historical-Era Warming in CESM2 Driven by Prescribed Biomass Burning Emissions. *Geophysical Research Letters*, e2021GL097420. Retrieved from `https://agupubs.onlinelibrary.wiley.com/doi/10.1029/2021GL097420` doi: 10.1029/2021GL097420

Flato, G., Marotzke, J., Abiodun, B., Braconnot, P., Chou, S., Collins, W., ... Rummukainen, M. (2013). IPCC AR5 - Chapter 9: Evaluation of Climate Models. *Climate Change 2013: The Physical Science Basis. Contribution of Working Group I to the Fifth Assessment Report of the Intergovernmental Panel on Climate Change*, 741–866.

Fyfe, J. C., Gillett, N. P., & Zwiers, F. W. (2013, aug). Overestimated global warming over the past 20 years. *Nature Climate Change*, *3*(9), 767–769. Retrieved from https://www.nature.com/articles/nclimate1972 doi: 10.1038/nclimate1972

Fyfe, J. C., Meehl, G. A., England, M. H., Mann, M. E., Santer, B. D., Flato, G. M., ... Swart, N. C. (2016, feb). Making sense of the early-2000s warming slowdown. *Nature Climate Change*, *6*(3), 224–228. Retrieved from https://www.nature.com/articles/nclimate2938 doi: 10.1038/nclimate2938

Fyfe, J. C., Merryfield, W. J., Kharin, V., Boer, G. J., Lee, W.-S., & von Salzen, K. (2011, nov). Skillful predictions of decadal trends in global mean surface temperature. *Geophysical Research Letters*, *38*(22), 22801. Retrieved from https://agupubs.onlinelibrary.wiley.com/doi/10.1029/2011GL049508 doi: 10.1029/2011GL049508

Gibson, P. B., Chapman, W. E., Altinok, A., Delle Monache, L., DeFlorio, M. J., & Waliser, D. E. (2021, aug). Training machine learning models on climate model output yields skillful interpretable seasonal precipitation forecasts. *Communications Earth & Environment*, *2*(1), 1–13. Retrieved from https://www.nature.com/articles/s43247-021-00225-4 doi: 10.1038/s43247-021-00225-4

Gordon, E. M., Barnes, E. A., & Hurrell, J. W. (2021, nov). Oceanic Harbingers of Pacific Decadal Oscillation Predictability in CESM2 Detected by Neural Networks. *Geophysical Research Letters*, *48*(21), e2021GL095392. Retrieved from https://agupubs.onlinelibrary.wiley.com/doi/10.1029/2021GL095392 doi: 10.1029/2021GL095392

Graham, R. J., Yun, W.-T., Kim, J., Kumar, A., Jones, D., Bettio, L., ... Smith, D. (2011, mar). Long-range forecasting and the Global Framework for Climate Services. *Climate Research*, *47*(1-2), 47–55. Retrieved from https://www.int-res.com/abstracts/cr/v47/n1-2/p47-55/ doi:

10.3354/CR00963

Guemas, V., Doblas-Reyes, F. J., Andreu-Burillo, I., & Asif, M. (2013, apr). Retrospective prediction of the global warming slowdown in the past decade. *Nature Climate Change*, *3*(7), 649–653. Retrieved from https://www.nature.com/articles/nclimate1863 doi: 10.1038/nclimate1863

Ham, Y.-G., Kim, J.-H., & Luo, J.-J. (2019, sep). Deep learning for multi-year ENSO forecasts. *Nature =*, *573*(7775), 568–572. Retrieved from https://www.nature.com/articles/s41586-019-1559-7 doi: 10.1038/s41586-019-1559-7

Hansen, J., Ruedy, R., Sato, M., & Lo, K. (2010, dec). GLOBAL SURFACE TEMPERATURE CHANGE. *Reviews of Geophysics*, *48*(4), 4004. Retrieved from https://agupubs.onlinelibrary.wiley.com/doi/10.1029/2010RG000345 doi: 10.1029/2010RG000345

Hawkins, E., Frame, D., Harrington, L., Joshi, M., King, A., Rojas, M., & Sutton, R. (2020, mar). Observed Emergence of the Climate Change Signal: From the Familiar to the Unknown. *Geophysical Research Letters*, *47*(6). Retrieved from https://onlinelibrary.wiley.com/doi/abs/10.1029/2019GL086259 doi: 10.1029/2019GL086259

Hedemann, C., Mauritsen, T., Jungclaus, J., & Marotzke, J. (2017, apr). The subtle origins of surface-warming hiatuses. *Nature Climate Change 2017 7:5*, *7*(5), 336–339. Retrieved from https://www.nature.com/articles/nclimate3274 doi: 10.1038/nclimate3274

Henley, B. J., Gergis, J., Karoly, D. J., Power, S., Kennedy, J., & Folland, C. K. (2015). A Tripole Index for the Interdecadal Pacific Oscillation. *Climate Dynamics*. doi: 10.1007/s00382-015-2525-1

Hersbach, H., Bell, B., Berrisford, P., Hirahara, S., Horányi, A., Muñoz-Sabater, J., ... Thépaut, J.-N. (2020, may). The ERA5 Global Reanalysis. *Quarterly Journal of the Royal Meteorological Society*. Retrieved from https://onlinelibrary.wiley.com/doi/abs/10.1002/qj.3803 doi: 10.1002/qj.3803

Hewitt, C. D., Guglielmo, F., Joussaume, S., Bessembinder, J., Christel, I., Doblas-Reyes, F. J., ... Clair, A. L. S. (2021, mar). Recommendations for Future Research Priorities for Climate Modeling and Climate Services. *Bul-*

letin of the American Meteorological Society, *102*(3), E578–E588. Retrieved from https://journals.ametsoc.org/view/journals/bams/102/3/BAMS-D-20-0103.1.xml doi: 10.1175/BAMS-D-20-0103.1

Irrgang, C., Boers, N., Sonnewald, M., Barnes, E. A., Kadow, C., Staneva, J., & Saynisch-Wagner, J. (2021, aug). Towards neural Earth system modelling by integrating artificial intelligence in Earth system science. *Nature Machine Intelligence*, *3*(8), 667–674. Retrieved from https://www.nature.com/articles/s42256-021-00374-3 doi: 10.1038/s42256-021-00374-3

Izumo, T., Vialard, J., Lengaigne, M., De Boyer Montegut, C., Behera, S. K., Luo, J. J., ... Yamagata, T. (2010, feb). Influence of the state of the Indian Ocean Dipole on the following year's El Niño. *Nature Geoscience*, *3*(3), 168–172. Retrieved from https://www.nature.com/articles/ngeo760 doi: 10.1038/ngeo760

Johnson, N. C., Amaya, D. J., Ding, Q., Kosaka, Y., Tokinaga, H., & Xie, S. P. (2020, may). Multidecadal modulations of key metrics of global climate change. *Global and Planetary Change*, *188*, 103149. doi: 10.1016/J.GLOPLACHA.2020.103149

Karl, T. R., Arguez, A., Huang, B., Lawrimore, J. H., McMahon, J. R., Menne, M. J., ... Zhang, H.-M. (2015, jun). Possible artifacts of data biases in the recent global surface warming hiatus. *Science*, *348*(6242), 1469–1472. Retrieved from https://www.science.org/doi/abs/10.1126/science.aaa5632 doi: 10.1126/SCIENCE.AAA5632

Kosaka, Y., & Xie, S.-P. (2013, aug). Recent global-warming hiatus tied to equatorial Pacific surface cooling. *Nature*, *501*(7467), 403–407. Retrieved from https://www.nature.com/articles/nature12534 doi: 10.1038/nature12534

Kushnir, Y., Scaife, A. A., Arritt, R., Balsamo, G., Boer, G., Doblas-Reyes, F., ... Wu, B. (2019, jan). Towards operational predictions of the near-term climate. *Nature Climate Change*, *9*(2), 94–101. Retrieved from https://www.nature.com/articles/s41558-018-0359-7 doi: 10.1038/s41558-018-0359-7

Labe, Z. M., & Barnes, E. A. (2021). Detecting climate signals using explainable AI with single-forcing large ensembles. *Journal of Advances in Modeling Earth*

Systems, *13*(6), 1–18. Retrieved from https://agupubs.onlinelibrary.wiley.com/doi/10.1029/2021MS002464 doi: 10.1029/2021MS002464

Le, T., Ha, K. J., Bae, D. H., & Kim, S. H. (2020, oct). Causal effects of Indian Ocean Dipole on El Niño–Southern Oscillation during 1950–2014 based on high-resolution models and reanalysis data. *Environmental Research Letters*, *15*(10), 1040b6. Retrieved from https://iopscience.iop.org/article/10.1088/1748-9326/abb96d/meta doi: 10.1088/1748-9326/ABB96D

Lewandowsky, S., Cowtan, K., Risbey, J. S., Mann, M. E., Steinman, B. A., Oreskes, N., & Rahmstorf, S. (2018, dec). The 'pause' in global warming in historical context: (II). Comparing models to observations. *Environmental Research Letters*, *13*(12), 123007. Retrieved from https://iopscience.iop.org/article/10.1088/1748-9326/aaf372/meta doi: 10.1088/1748-9326/AAF372

Lewandowsky, S., Risbey, J. S., & Oreskes, N. (2016, may). The "Pause" in Global Warming: Turning a Routine Fluctuation into a Problem for Science. *Bulletin of the American Meteorological Society*, *97*(5), 723–733. Retrieved from https://journals.ametsoc.org/view/journals/bams/97/5/bams-d-14-00106.1.xml doi: 10.1175/BAMS-D-14-00106.1

Li, T. W., & Baker, N. C. (2016, jul). Detecting Warming Hiatus Periods in CMIP5 Climate Model Projections. *International Journal of Atmospheric Sciences*, 1–7. doi: 10.1155/2016/9657659

Li-Jing, C., Jiang, Z., & Abraham, J. (2015, jan). Global Upper Ocean Heat Content Estimation: Recent Progress and the Remaining Challenges. *Atmospheric and Oceanic Science Letters*, *8*(6), 333–338. Retrieved from https://www.tandfonline.com/action/journalInformation?journalCode=taos20 doi: 10.3878/AOSL20150031

Liu, G., Wang, P., Beveridge, M., & Kwon, Y.-O. (2021). Predicting Atlantic Multidecadal Variability. *NeurIPS 2021 Workshop on Tackling Climate Change with Machine Learning*, 1–7. Retrieved from https://arxiv.org/abs/2111.00124

Liu, J., Tang, Y., Wu, Y., Li, T., Wang, Q., & Chen, D. (2021, oct). Forecasting the Indian Ocean Dipole With Deep Learning Techniques. *Geophysical Research Letters*, *48*(20), e2021GL094407. Retrieved from https://agupubs.onlinelibrary.wiley.com/doi/10.1029/2021GL094407 doi:

10.1029/2021GL094407

Liu, W., & Xie, S. P. (2018, jun). An ocean view of the global surface warming hiatus. *Oceanography*, *31*(2 Special Issue), 72–79. doi: 10.5670/OCEANOG.2018.217

Maher, N., Gupta, A. S., & England, M. H. (2014). *Drivers of decadal hiatus periods in the 20th and 21st centuries* (Vol. 41) (No. 16). doi: 10.1002/2014GL060527

Maher, N., Lehner, F., & Marotzke, J. (2020, may). Quantifying the role of internal variability in the temperature we expect to observe in the coming decades. *Environmental Research Letters*, *15*(5), 054014. Retrieved from https://iopscience.iop.org/article/10.1088/1748-9326/ab7d02/meta doi: 10.1088/1748-9326/AB7D02

Maher, N., Milinski, S., & Ludwig, R. (2021, apr). Large ensemble climate model simulations: introduction, overview, and future prospects for utilising multiple types of large ensemble. *Earth System Dynamics*, *12*(2), 401–418. Retrieved from https://esd.copernicus.org/articles/12/401/2021/ doi: 10.5194/esd-12-401-2021

Mamalakis, A., Ebert-Uphoff, I., & Barnes, E. A. (2021, mar). Neural Network Attribution Methods for Problems in Geoscience: A Novel Synthetic Benchmark Dataset. *arXiv*. Retrieved from http://arxiv.org/abs/2103.10005

Mann, M. E., Miller, S. K., Rahmstorf, S., Steinman, B. A., & Tingley, M. (2017, aug). Record temperature streak bears anthropogenic fingerprint. *Geophysical Research Letters*, *44*(15), 7936–7944. Retrieved from https://agupubs.onlinelibrary.wiley.com/doi/10.1002/2017GL074056 doi: 10.1002/2017GL074056

Mann, M. E., Steinman, B. A., Miller, S. K., Frankcombe, L. M., England, M. H., & Cheung, A. H. (2016, apr). Predictability of the recent slowdown and subsequent recovery of large-scale surface warming using statistical methods. *Geophysical Research Letters*, *43*(7), 3459–3467. Retrieved from https://agupubs.onlinelibrary.wiley.com/doi/10.1002/2016GL068159 doi: 10.1002/2016GL068159

Mayer, K. J., & Barnes, E. A. (2021, may). Subseasonal Forecasts of Opportunity Identified by an Explainable Neural Network. *Geophysical Research Let-*

ters, *48*(10), e2020GL092092. Retrieved from https://onlinelibrary.wiley.com/doi/10.1029/2020GL092092 doi: 10.1029/2020GL092092

McGovern, A., Lagerquist, R., Gagne, D. J., Jergensen, G. E., Elmore, K. L., Homeyer, C. R., & Smith, T. (2019, nov). Making the black box more transparent: Understanding the physical implications of machine learning. *Bulletin of the American Meteorological Society*, *100*(11), 2175–2199. Retrieved from http://journals.ametsoc.org/bams/article-pdf/100/11/2175/4876688/bams-d-18-0195{_}1.pdf doi: 10.1175/BAMS-D-18-0195.1

Medhaug, I., Stolpe, M. B., Fischer, E. M., & Knutti, R. (2017, may). Reconciling controversies about the 'global warming hiatus'. *Nature*, *545*(7652), 41–47. Retrieved from https://www.nature.com/articles/nature22315 doi: 10.1038/nature22315

Meehl, G. A., Arblaster, J. M., Fasullo, J. T., Hu, A., & Trenberth, K. E. (2011, sep). Model-based evidence of deep-ocean heat uptake during surface-temperature hiatus periods. *Nature Climate Change*, *1*(7), 360–364. Retrieved from https://www.nature.com/articles/nclimate1229 doi: 10.1038/nclimate1229

Meehl, G. A., Goddard, L., Boer, G., Burgman, R., Branstator, G., Cassou, C., ... Yeager, S. (2013). Decadal Climate Prediction: An Update from the Trenches. *Bulletin of the American Meteorological Society*. Retrieved from http://dx.doi.org/10.1175/BAMS-D-12-00241.1 doi: 10.1175/BAMS-D-12-00241.1

Meehl, G. A., Hu, A., Arblaster, J. M., Fasullo, J., & Trenberth, K. E. (2013, sep). Externally Forced and Internally Generated Decadal Climate Variability Associated with the Interdecadal Pacific Oscillation. *Journal of Climate*, *26*(18), 7298–7310. Retrieved from https://journals.ametsoc.org/view/journals/clim/26/18/jcli-d-12-00548.1.xml doi: 10.1175/JCLI-D-12-00548.1

Meehl, G. A., Richter, J. H., Teng, H., Capotondi, A., Cobb, K., Doblas-Reyes, F., ... Xie, S.-P. (2021, apr). Initialized Earth System prediction from subseasonal to decadal timescales. *Nature Reviews Earth & Environment*, *2*(5), 340–357. Retrieved from https://www.nature.com/articles/s43017-021-00155-x doi: 10.1038/s43017-021-00155-x

Meehl, G. A., & Teng, H. (2014, mar). CMIP5 multi-model hindcasts for the

694 mid-1970s shift and early 2000s hiatus and predictions for 2016–2035. *Geo-*
695 *physical Research Letters*, *41*(5), 1711–1716. Retrieved from `https://`
696 `agupubs.onlinelibrary.wiley.com/doi/10.1002/2014GL059256` doi:
697 10.1002/2014GL059256

698 Meehl, G. A., Teng, H., & Arblaster, J. M. (2014, sep). Climate model simula-
699 tions of the observed early-2000s hiatus of global warming. *Nature Climate*
700 *Change*, *4*(10), 898–902. Retrieved from `https://www.nature.com/articles/`
701 `nclimate2357` doi: 10.1038/nclimate2357

702 Merryfield, W. J., Baehr, J., Batté, L., Becker, E. J., Butler, A. H., Coelho,
703 C. A. S., ... Yeager, S. (2020, jun). Current and Emerging Develop-
704 ments in Subseasonal to Decadal Prediction. *Bulletin of the American*
705 *Meteorological Society*, *101*(6), E869–E896. Retrieved from `https://`
706 `journals.ametsoc.org/view/journals/bams/101/6/bamsD190037.xml`
707 doi: 10.1175/BAMS-D-19-0037.1

708 Modak, A., & Mauritsen, T. (2021, may). The 2000–2012 Global Warming Hiatus
709 More Likely With a Low Climate Sensitivity. *Geophysical Research Letters*,
710 *48*(9), e2020GL091779. Retrieved from `https://onlinelibrary.wiley.com/`
711 `doi/full/10.1029/2020GL091779https://onlinelibrary.wiley.com/doi/`
712 `abs/10.1029/2020GL091779https://agupubs.onlinelibrary.wiley.com/`
713 `doi/10.1029/2020GL091779` doi: 10.1029/2020GL091779

714 Montavon, G., Lapuschkin, S., Binder, A., Samek, W., & Müller, K. R. (2017, may).
715 Explaining nonlinear classification decisions with deep Taylor decomposition.
716 *Pattern Recognition*, *65*, 211–222. doi: 10.1016/j.patcog.2016.11.008

717 Montavon, G., Samek, W., & Müller, K. R. (2018, feb). *Methods for interpreting and*
718 *understanding deep neural networks* (Vol. 73). Elsevier Inc. doi: 10.1016/j.dsp
719 .2017.10.011

720 Nadiga, B. T. (2021, apr). Reservoir Computing as a Tool for Climate Pre-
721 dictability Studies. *Journal of Advances in Modeling Earth Systems*, *13*(4),
722 e2020MS002290. Retrieved from `https://agupubs.onlinelibrary.wiley`
723 `.com/doi/10.1029/2020MS002290` doi: 10.1029/2020MS002290

724 Newman, M., Alexander, M. A., Ault, T. R., Cobb, K. M., Deser, C., Di Lorenzo,
725 E., ... Smith, C. A. (2016, jun). The Pacific Decadal Oscillation,
726 Revisited. *Journal of Climate*, *29*(12), 4399–4427. Retrieved from

http://journals.ametsoc.org/doi/10.1175/JCLI-D-15-0508.1 doi: 10.1175/JCLI-D-15-0508.1

O'Neill, B. C., Tebaldi, C., Van Vuuren, D. P., Eyring, V., Friedlingstein, P., Hurtt, G., ... Sanderson, B. M. (2016, sep). The Scenario Model Intercomparison Project (ScenarioMIP) for CMIP6. *Geoscientific Model Development*, *9*(9), 3461–3482. doi: 10.5194/GMD-9-3461-2016

Papalexiou, S. M., Rajulapati, C. R., Clark, M. P., & Lehner, F. (2020, oct). Robustness of CMIP6 Historical Global Mean Temperature Simulations: Trends, Long-Term Persistence, Autocorrelation, and Distributional Shape. *Earth's Future*, *8*(10), e2020EF001667. Retrieved from https://agupubs.onlinelibrary.wiley.com/doi/10.1029/2020EF001667 doi: 10.1029/2020EF001667

Parker, D., Folland, C., Scaife, A., Knight, J., Colman, A., Baines, P., & Dong, B. (2007, sep). Decadal to multidecadal variability and the climate change background. *Journal of Geophysical Research: Atmospheres*, *112*(D18), 18115. Retrieved from https://agupubs.onlinelibrary.wiley.com/doi/10.1029/2007JD008411 doi: 10.1029/2007JD008411

Phillips, A. S., Deser, C., Fasullo, J., Schneider, D. P., & Simpson, I. R. (2020). *Assessing Climate Variability and Change in Model Large Ensembles: A User's Guide to the Climate Variability Diagnostics Package for Large Ensembles Version 1.0* (Tech. Rep.). Boulder, Colorado: NCAR. Retrieved from https://opensky.ucar.edu/islandora/object/manuscripts:1001 doi: 10.5065/h7c7-f961

Power, S., Lengaigne, M., Capotondi, A., Khodri, M., Vialard, J., Jebri, B., ... Henley, B. J. (2021, oct). Decadal climate variability in the tropical Pacific: Characteristics, causes, predictability, and prospects. *Science*, *374*(6563). Retrieved from https://www.science.org/doi/abs/10.1126/science.aay9165 doi: 10.1126/SCIENCE.AAY9165

Reichstein, M., Camps-Valls, G., Stevens, B., Jung, M., Denzler, J., Carvalhais, N., & Prabhat. (2019, feb). Deep learning and process understanding for data-driven Earth system science. *Nature*, *566*(7743), 195–204. Retrieved from https://www.nature.com/articles/s41586-019-0912-1 doi: 10.1038/s41586-019-0912-1

Risbey, J. S., Lewandowsky, S., Cowtan, K., Oreskes, N., Rahmstorf, S., Jokimäki, A., & Foster, G. (2018, dec). A fluctuation in surface temperature in historical context: reassessment and retrospective on the evidence. *Environmental Research Letters*, *13*(12), 123008. Retrieved from https://iopscience.iop.org/article/10.1088/1748-9326/aaf342/meta doi: 10.1088/1748-9326/AAF342

Roberts, C. D., Palmer, M. D., McNeall, D., & Collins, M. (2015, feb). Quantifying the likelihood of a continued hiatus in global warming. *Nature Climate Change*, *5*(4), 337–342. Retrieved from https://www.nature.com/articles/nclimate2531 doi: 10.1038/nclimate2531

Rodgers, K., Lee, S.-S., Rosenbloom, N., Timmermann, A., Danabasoglu, G., Deser, C., ... Yeager, S. (2021). Ubiquity of human-induced changes in climate variability. *Earth System Dynamics Discussions*, 1–22. doi: 10.5194/ESD-2021-50

Saji, N. H., Goswami, B. N., Vinayachandran, P. N., & Yamagata, T. (1999, sep). A dipole mode in the tropical Indian Ocean. *Nature 1999*, *401*(6751), 360–363. Retrieved from https://www.nature.com/articles/43854 doi: 10.1038/43854

Santer, B. D., Bonfils, C., Painter, J. F., Zelinka, M. D., Mears, C., Solomon, S., ... Wentz, F. J. (2014, feb). Volcanic contribution to decadal changes in tropospheric temperature. *Nature Geoscience 2014 7:3*, *7*(3), 185–189. Retrieved from https://www.nature.com/articles/ngeo2098 doi: 10.1038/ngeo2098

Santoso, A., Mcphaden, M. J., & Cai, W. (2017, dec). The Defining Characteristics of ENSO Extremes and the Strong 2015/2016 El Niño. *Reviews of Geophysics*, *55*(4), 1079–1129. Retrieved from https://agupubs.onlinelibrary.wiley.com/doi/10.1002/2017RG000560 doi: 10.1002/2017RG000560

Schmidt, G. A., Shindell, D. T., & Tsigaridis, K. (2014, feb). Reconciling warming trends. *Nature Geoscience*, *7*(3), 158–160. Retrieved from https://www.nature.com/articles/ngeo2105 doi: 10.1038/ngeo2105

Sévellec, F., & Drijfhout, S. S. (2018, aug). A novel probabilistic forecast system predicting anomalously warm 2018-2022 reinforcing the long-term global warming trend. *Nature Communications*, *9*(1), 1–12. Retrieved from https://www.nature.com/articles/s41467-018-05442-8 doi: 10.1038/s41467-018-05442-8

Sévellec, F., Sinha, B., & Skliris, N. (2016, aug). The rogue nature of hiatuses in a global warming climate. *Geophysical Research Letters*, *43*(15), 8169–8177. Retrieved from https://agupubs.onlinelibrary.wiley.com/doi/10.1002/2016GL068950 doi: 10.1002/2016GL068950

Smith, D. M., Booth, B. B., Dunstone, N. J., Eade, R., Hermanson, L., Jones, G. S., ... Thompson, V. (2016). Role of volcanic and anthropogenic aerosols in the recent global surface warming slowdown. *Nature Climate Change*, *6*(10). doi: 10.1038/nclimate3058

Smith, D. M., Eade, R., Scaife, A. A., Caron, L.-P., Danabasoglu, G., DelSole, T. M., ... Yang, X. (2019, may). Robust skill of decadal climate predictions. *npj Climate and Atmospheric Science 2019 2:1*, *2*(1), 1–10. Retrieved from https://www.nature.com/articles/s41612-019-0071-y doi: 10.1038/s41612-019-0071-y

Sonnewald, M., & Lguensat, R. (2021, aug). Revealing the Impact of Global Heating on North Atlantic Circulation Using Transparent Machine Learning. *Journal of Advances in Modeling Earth Systems*, *13*(8), e2021MS002496. Retrieved from https://agupubs.onlinelibrary.wiley.com/doi/10.1029/2021MS002496 doi: 10.1029/2021MS002496

Sonnewald, M., Lguensat, R., Jones, D. C., Dueben, P. D., Brajard, J., & Balaji, V. (2021, jul). Bridging observations, theory and numerical simulation of the ocean using machine learning. *Environmental Research Letters*, *16*(7), 073008. Retrieved from https://iopscience.iop.org/article/10.1088/1748-9326/ac0eb0/meta doi: 10.1088/1748-9326/AC0EB0

Tang, Y., & Duan, A. (2021, oct). Using deep learning to predict the East Asian summer monsoon. *Environmental Research Letters*. Retrieved from https://iopscience.iop.org/article/10.1088/1748-9326/ac34bc/meta doi: 10.1088/1748-9326/AC34BC

Thompson, D. W. J., Wallace, J. M., Jones, P. D., & Kennedy, J. J. (2009, nov). Identifying Signatures of Natural Climate Variability in Time Series of Global-Mean Surface Temperature: Methodology and Insights. *Journal of Climate*, *22*(22), 6120–6141. Retrieved from https://journals.ametsoc.org/view/journals/clim/22/22/2009jcli3089.1.xml doi: 10.1175/2009JCLI3089.1

Titchner, H. A., & Rayner, N. A. (2014, mar). The Met Office Hadley Centre

sea ice and sea surface temperature data set, version 2: 1. Sea ice concentrations. *Journal of Geophysical Research: Atmospheres*, *119*(6), 2864–2889. Retrieved from https://agupubs.onlinelibrary.wiley.com/doi/10.1002/2013JD020316 doi: 10.1002/2013JD020316

Toms, B. A., Barnes, E. A., & Ebert-Uphoff, I. (2020, sep). Physically Interpretable Neural Networks for the Geosciences: Applications to Earth System Variability. *Journal of Advances in Modeling Earth Systems*, *12*(9). Retrieved from https://onlinelibrary.wiley.com/doi/10.1029/2019MS002002 doi: 10.1029/2019MS002002

Toms, B. A., Barnes, E. A., & Hurrell, J. W. (2021, jun). Assessing Decadal Predictability in an Earth-System Model Using Explainable Neural Networks. *Geophysical Research Letters*, *48*(12), e2021GL093842. Retrieved from https://agupubs.onlinelibrary.wiley.com/doi/10.1029/2021GL093842 doi: 10.1029/2021GL093842

Trenberth, K. E., Caron, J. M., Stepaniak, D. P., & Worley, S. (2002, apr). Evolution of El Niño–Southern Oscillation and global atmospheric surface temperatures. *Journal of Geophysical Research: Atmospheres*, *107*(D8), AAC 5–1. Retrieved from https://agupubs.onlinelibrary.wiley.com/doi/10.1029/2000JD000298 doi: 10.1029/2000JD000298

Van Marle, M. J., Kloster, S., Magi, B. I., Marlon, J. R., Daniau, A. L., Field, R. D., ... Van Der Werf, G. R. (2017, sep). Historic global biomass burning emissions for CMIP6 (BB4CMIP) based on merging satellite observations with proxies and fire models (1750-2015). *Geoscientific Model Development*, *10*(9), 3329–3357. doi: 10.5194/GMD-10-3329-2017

von Känel, L., Frölicher, T. L., & Gruber, N. (2017, aug). Hiatus-like decades in the absence of equatorial Pacific cooling and accelerated global ocean heat uptake. *Geophysical Research Letters*, *44*(15), 7909–7918. Retrieved from https://agupubs.onlinelibrary.wiley.com/doi/10.1002/2017GL073578 doi: 10.1002/2017GL073578

Watanabe, M., Kamae, Y., Yoshimori, M., Oka, A., Sato, M., Ishii, M., ... Kimoto, M. (2013, jun). Strengthening of ocean heat uptake efficiency associated with the recent climate hiatus. *Geophysical Research Letters*, *40*(12), 3175–3179. Retrieved from https://agupubs.onlinelibrary.wiley.com/doi/10.1002/

grl.50541 doi: 10.1002/GRL.50541

Wei, M., Song, Z., Shu, Q., Yang, X., Song, Y., & Qiao, F. (2021, dec). Revisiting the existence of the global warming slowdown during the early 21st century. *Journal of Climate*, *-1*(aop), 1–40. Retrieved from https://journals-ametsoc-org.ezproxy2.library.colostate.edu/view/journals/clim/aop/JCLI-D-21-0373.1/JCLI-D-21-0373.1.xml doi: 10.1175/JCLI-D-21-0373.1

Wu, A., & Hsieh, W. W. (2004, jan). The nonlinear Northern Hemisphere winter atmospheric response to ENSO. *Geophysical Research Letters*, *31*(2). Retrieved from https://agupubs.onlinelibrary.wiley.com/doi/10.1029/2003GL018885 doi: 10.1029/2003GL018885

Xie, S.-P., & Kosaka, Y. (2017, mar). What Caused the Global Surface Warming Hiatus of 1998–2013? *Current Climate Change Reports 2017 3:2*, *3*(2), 128–140. Retrieved from https://link.springer.com/article/10.1007/s40641-017-0063-0 doi: 10.1007/S40641-017-0063-0

Yoo, J. H., Moon, S., Ha, K. J., Yun, K. S., & Lee, J. Y. (2020, aug). Cases for the sole effect of the Indian Ocean Dipole in the rapid phase transition of the El Niño–Southern Oscillation. *Theoretical and Applied Climatology*, *141*(3-4), 999–1007. Retrieved from https://link.springer.com/article/10.1007/s00704-020-03265-6 doi: 10.1007/S00704-020-03265-6/FIGURES/8

Zhang, C., Li, S., Luo, F., & Huang, Z. (2019, oct). The global warming hiatus has faded away: An analysis of 2014–2016 global surface air temperatures. *International Journal of Climatology*, *39*(12), 4853–4868. Retrieved from https://rmets.onlinelibrary.wiley.com/doi/10.1002/joc.6114 doi: 10.1002/JOC.6114

References From the Supporting Information

Abadi, M., Barham, P., Chen, J., Chen, Z., Davis, A., Dean, J., ... Zheng, X. (2016). TensorFlow: A system for large-scale machine learning. In *Proceedings of the 12th usenix symposium on operating systems design and implementation, osdi 2016.*

Agarap, A. F. (2018, mar). Deep Learning using Rectified Linear Units (ReLU). *arXiv*. Retrieved from http://arxiv.org/abs/1803.08375

A.Géron. (2019). *Hands-on machine learning with Scikit-Learn, Keras and TensorFlow: concepts, tools, and techniques to build intelligent systems.*

Alber, M., Lapuschkin, S., Seegerer, P., Hägele, M., Schütt, K. T., Montavon, G., ... Kindermans, P. J. (2019). INNvestigate neural networks! *Journal of Machine Learning Research*, *20*.

Bach, S., Binder, A., Montavon, G., Klauschen, F., Müller, K. R., & Samek, W. (2015, jul). On pixel-wise explanations for non-linear classifier decisions by layer-wise relevance propagation. *PLoS ONE*, *10*(7), e0130140. Retrieved from http://www.hfsp.org/, doi: 10.1371/journal.pone.0130140

Boukabara, S.-A., Krasnopolsky, V., Penny, S. G., Stewart, J. Q., McGovern, A., Hall, D., ... Hoffman, R. N. (2021, may). Outlook for Exploiting Artificial Intelligence in the Earth and Environmental Sciences. *Bulletin of the American Meteorological Society*, *102*(5), E1016–E1032. Retrieved from https://journals.ametsoc.org/view/journals/bams/102/5/BAMS-D-20-0031.1.xml doi: 10.1175/BAMS-D-20-0031.1

Capotondi, A., Deser, C., Phillips, A. S., Okumura, Y., & Larson, S. M. (2020, dec). ENSO and Pacific Decadal Variability in the Community Earth System Model Version 2. *Journal of Advances in Modeling Earth Systems*, *12*(12), e2019MS002022. Retrieved from https://agupubs.onlinelibrary.wiley.com/doi/10.1029/2019MS002022 doi: 10.1029/2019MS002022

Chen, H.-C., Fei-Fei-Jin, Zhao, S., Wittenberg, A. T., & Xie, S. (2021, dec). ENSO Dynamics in the E3SM-1-0, CESM2, and GFDL-CM4 Climate Models. *Journal of Climate*, *34*(23), 9365–9384. Retrieved from https://journals.ametsoc.org/view/journals/clim/34/23/JCLI-D-21-0355.1.xml doi: 10.1175/JCLI-D-21-0355.1

Crameri, F. (2018, jan). Scientific colour maps. *Zenodo*. Retrieved from https://zenodo.org/record/4153113 doi: 10.5281/ZENODO.4153113

Crameri, F., Shephard, G. E., & Heron, P. J. (2020, dec). The misuse of colour in science communication. *Nature Communications*, *11*(1), 1–10. Retrieved from https://doi.org/10.1038/s41467-020-19160-7 doi: 10.1038/s41467-020-19160-7

Danabasoglu, G., Bates, S. C., Briegleb, B. P., Jayne, S. R., Jochum, M., Large, W. G., ... Yeager, S. G. (2012). The CCSM4 ocean component. *Journal of*

Climate, *25*(5). doi: 10.1175/JCLI-D-11-00091.1

Danabasoglu, G., Lamarque, J.-F., Bacmeister, J., Bailey, D. A., DuVivier, A. K., Edwards, J., ... Strand, W. G. (2020, feb). The Community Earth System Model Version 2 (CESM2). *Journal of Advances in Modeling Earth Systems*, *12*(2), e2019MS001916. Retrieved from `https://agupubs.onlinelibrary.wiley.com/doi/10.1029/2019MS001916` doi: 10.1029/2019MS001916

Fasullo, J. T. (2020, aug). Evaluating simulated climate patterns from the CMIP archives using satellite and reanalysis datasets using the Climate Model Assessment Tool (CMATv1). *Geoscientific Model Development*, *13*(8), 3627–3642. doi: 10.5194/GMD-13-3627-2020

Friedman, J. H. (2012, jul). Fast sparse regression and classification. *International Journal of Forecasting*, *28*(3), 722–738. doi: 10.1016/j.ijforecast.2012.05.001

Gettelman, A., Hannay, C., Bacmeister, J. T., Neale, R. B., Pendergrass, A. G., Danabasoglu, G., ... Mills, M. J. (2019, jul). High Climate Sensitivity in the Community Earth System Model Version 2 (CESM2). *Geophysical Research Letters*, *46*(14), 8329–8337. Retrieved from `https://agupubs.onlinelibrary.wiley.com/doi/10.1029/2019GL083978` doi: 10.1029/2019GL083978

Goodfellow, I., Bengio, Y., & Courville, A. (2016). *Deep Learning*.

Green, D. A. (2011). A colour scheme for the display of astronomical intensity images. *Bulletin of the Astronomical Society of India*, *39*(2).

Hansen, J., Ruedy, R., Sato, M., & Lo, K. (2010, dec). GLOBAL SURFACE TEMPERATURE CHANGE. *Reviews of Geophysics*, *48*(4), 4004. Retrieved from `https://agupubs.onlinelibrary.wiley.com/doi/10.1029/2010RG000345` doi: 10.1029/2010RG000345

Harris, C. R., Jarrod Millman, K., van der Walt, S. J., Gommers, R., Virtanen, P., Cournapeau, D., ... Oliphant, T. E. (2020, sep). Array programming with NumPy. *Nature*, *585*(7825), 357. Retrieved from `https://doi.org/10.1038/s41586-020-2649-2` doi: 10.1038/s41586-020-2649-2

Henley, B. J., Gergis, J., Karoly, D. J., Power, S., Kennedy, J., & Folland, C. K. (2015). A Tripole Index for the Interdecadal Pacific Oscillation. *Climate Dynamics*. doi: 10.1007/s00382-015-2525-1

Hersbach, H., Bell, B., Berrisford, P., Hirahara, S., Horányi, A., Muñoz-Sabater, J., ... Thépaut, J.-N. (2020, may). The ERA5 Global Reanalysis. *Quarterly Journal of the Royal Meteorological Society*. Retrieved from https://onlinelibrary.wiley.com/doi/abs/10.1002/qj.3803 doi: 10.1002/qj.3803

Hunter, J. D. (2007, may). Matplotlib: A 2D graphics environment. *Computing in Science and Engineering*, *9*(3), 99–104. doi: 10.1109/MCSE.2007.55

Hurrell, J. W., Holland, M. M., Gent, P. R., Ghan, S., Kay, J. E., Kushner, P. J., ... Marshall, S. (2013). The community earth system model: A framework for collaborative research. *Bulletin of the American Meteorological Society*, *94*(9). doi: 10.1175/BAMS-D-12-00121.1

Johnson, J. M., & Khoshgoftaar, T. M. (2019). Survey on deep learning with class imbalance. *Journal of Big Data*, *6*(1). doi: 10.1186/s40537-019-0192-5

Kanamitsu, M., Ebisuzaki, W., Woollen, J., Yang, S.-K., Hnilo, J. J., Fiorino, M., & Potter, G. L. (2002, nov). NCEP–DOE AMIP-II Reanalysis (R-2). *Bulletin of the American Meteorological Society*, *83*(11), 1631–1643. Retrieved from http://journals.ametsoc.org/doi/abs/10.1175/BAMS-83-11-1631 doi: 10.1175/BAMS-83-11-1631

Kay, J. E., Deser, C., Phillips, A., Mai, A., Hannay, C., Strand, G., ... Vertenstein, M. (2015, aug). The Community Earth System Model (CESM) Large Ensemble Project: A Community Resource for Studying Climate Change in the Presence of Internal Climate Variability. *Bulletin of the American Meteorological Society*, *96*(8), 1333–1349. Retrieved from http://journals.ametsoc.org/doi/10.1175/BAMS-D-13-00255.1 doi: 10.1175/BAMS-D-13-00255.1

Lecun, Y., Bengio, Y., & Hinton, G. (2015, may). *Deep learning* (Vol. 521) (No. 7553). Nature Publishing Group. Retrieved from https://www.nature.com/articles/nature14539 doi: 10.1038/nature14539

Lee, J., Planton, Y. Y., Gleckler, P. J., Sperber, K. R., Guilyardi, E., Wittenberg, A. T., ... Pallotta, G. (2021, oct). Robust Evaluation of ENSO in Climate Models: How Many Ensemble Members Are Needed? *Geophysical Research Letters*, *48*(20), e2021GL095041. Retrieved from https://agupubs-onlinelibrary-wiley-com.ezproxy2.library.colostate.edu

990 doi: 10.1029/2021GL095041

991 Lenssen, N. J. L., Schmidt, G. A., Hansen, J. E., Menne, M. J., Persin, A., Ruedy,
992 R., & Zyss, D. (2019, jun). Improvements in the GISTEMP Uncertainty
993 Model. *Journal of Geophysical Research: Atmospheres*, *124*(12), 6307–6326.
994 Retrieved from `https://onlinelibrary.wiley.com/doi/abs/10.1029/`
995 `2018JD029522` doi: 10.1029/2018JD029522

996 Meehl, G. A., Arblaster, J. M., Bates, S., Richter, J. H., Tebaldi, C., Gettelman,
997 A., ... Strand, G. (2020, sep). Characteristics of Future Warmer Base States
998 in CESM2. *Earth and Space Science*, *7*(9), e2020EA001296. Retrieved from
999 `https://agupubs.onlinelibrary.wiley.com/doi/10.1029/2020EA001296`
1000 doi: 10.1029/2020EA001296

1001 Montavon, G., Samek, W., & Müller, K. R. (2018, feb). *Methods for interpreting and*
1002 *understanding deep neural networks* (Vol. 73). Elsevier Inc. doi: 10.1016/j.dsp
1003 .2017.10.011

1004 Morice, C. P., Kennedy, J. J., Rayner, N. A., Winn, J. P., Hogan, E., Killick, R. E.,
1005 ... Simpson, I. R. (2021, feb). An Updated Assessment of Near-Surface
1006 Temperature Change From 1850: The HadCRUT5 Data Set. *Journal of Geo-*
1007 *physical Research: Atmospheres*, *126*(3), e2019JD032361. Retrieved from
1008 `https://agupubs.onlinelibrary.wiley.com/doi/10.1029/2019JD032361`
1009 doi: 10.1029/2019JD032361

1010 NCAR. (2019). *The NCAR Command Language (Version 6.6.2).* Boulder, Col-
1011 orado. Retrieved from `http://dx.doi.org/10.5065/D6WD3XH5` doi: http://
1012 dx.doi.org/10.5065/D6WD3XH5

1013 Neapolitan, R. E., & Jiang, X. (2018, nov). Neural Networks and Deep Learning. In
1014 *Artificial intelligence* (pp. 389–411). Chapman and Hall/CRC. doi: 10.1201/
1015 b22400-15

1016 Nesterov, Y. (1983). A method for unconstrained convex minimization problem with
1017 the rate of convergence o(1/kˆ2). *Doklady AN USSR*, *269*.

1018 Pedregosa, F., Varoquaux, G., Gramfort, A., Michel, V., Thirion, B., Grisel, O., ...
1019 Duchesnay, É. (2011). Scikit-learn: Machine learning in Python. *Journal of*
1020 *Machine Learning Research*, *12*.

1021 Rohde, R. A., & Hausfather, Z. (2020, dec). The Berkeley Earth Land/Ocean
1022 Temperature Record. *Earth System Science Data*, *12*(4), 3469–3479. Re-

trieved from https://essd.copernicus.org/articles/12/3469/2020/ doi: 10.5194/essd-12-3469-2020

Ruder, S. (2016, sep). An overview of gradient descent optimization algorithms. *arXiv*. Retrieved from http://arxiv.org/abs/1609.04747

Schulzweida, U. (2019, feb). CDO User Guide. *Zenodo*. Retrieved from https://zenodo.org/record/2558193 doi: 10.5281/ZENODO.2558193

Shultz, T. R., & Fahlman, S. E. (2017). Confusion Matrix. *Encyclopedia of Machine Learning and Data Mining*, 260–260. Retrieved from https://link.springer.com/referenceworkentry/10.1007/978-1-4899-7687-1{_}50 doi: 10.1007/978-1-4899-7687-1_50

Smith, R., Jones, P., Briegleb, B., Bryan, F., Danabasoglu, G., Dennis, J., ... Yeager, S. (2010). The Parallel Ocean Program (POP) reference manual: Ocean component of the Community Climate System Model (CCSM). *Rep. LAUR-01853*, *141*.

Thyng, K., Greene, C., Hetland, R., Zimmerle, H., & DiMarco, S. (2016, sep). True Colors of Oceanography: Guidelines for Effective and Accurate Colormap Selection. *Oceanography*, *29*(3), 9–13. Retrieved from https://tos.org/oceanography/article/true-colors-of-oceanography-guidelines-for-effective-and-accurate-colormap doi: 10.5670/oceanog.2016.66

Virtanen, P., Gommers, R., Oliphant, T. E., Haberland, M., Reddy, T., Cournapeau, D., ... Vázquez-Baeza, Y. (2020). SciPy 1.0: fundamental algorithms for scientific computing in Python. *Nature Methods*, *17*(3). doi: 10.1038/s41592-019-0686-2

Zender, C. S. (2008). Analysis of self-describing gridded geoscience data with netCDF Operators (NCO). *Environmental Modelling and Software*, *23*(10-11). doi: 10.1016/j.envsoft.2008.03.004

Figure 1.

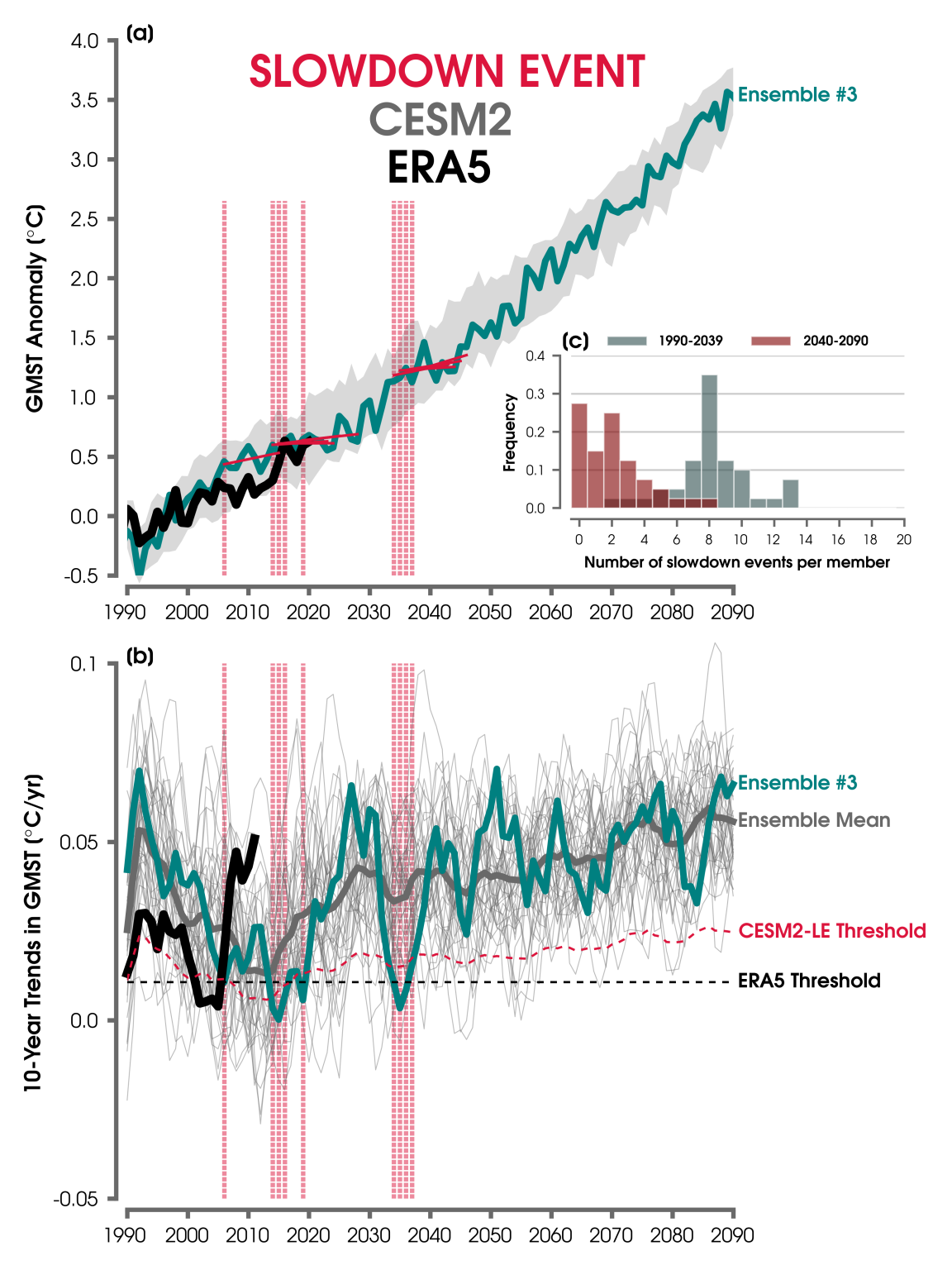
(a)
SLOWDOWN EVENT
CESM2
ERA5
Ensemble #3
GMST Anomaly (°C)
4.0
3.5
3.0
2.5
2.0
1.5
1.0
0.5
0.0
-0.5
1990
2000
2010
2020
2030
2040
2050
2060
2070
2080
2090
(c)
1990-2039
2040-2090
Frequency
0.4
0.3
0.2
0.1
0.0
0
2
4
6
8
10
12
14
16
18
20
Number of slowdown events per member
(b)
10-Year Trends in GMST (°C/yr)
0.1
0.05
0.0
-0.05
Ensemble #3
Ensemble Mean
CESM2-LE Threshold
ERA5 Threshold

Figure 2.

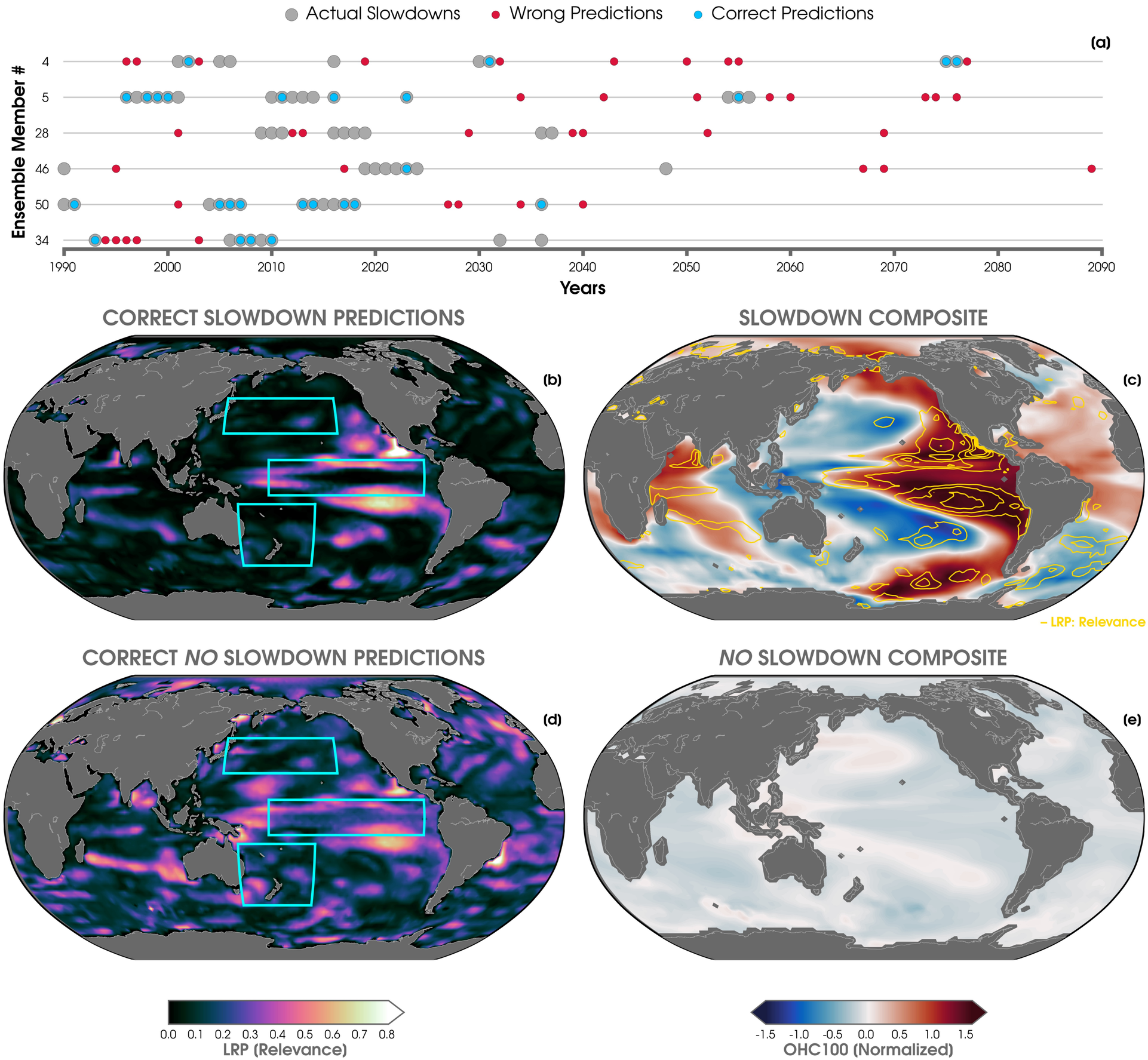
Actual Slowdowns
Wrong Predictions
Correct Predictions
(a)
Ensemble Member #
4
5
28
46
50
34
1990
2000
2010
2020
2030
2040
2050
2060
2070
2080
2090
Years
CORRECT SLOWDOWN PREDICTIONS
SLOWDOWN COMPOSITE
(b)
(c)
– LRP: Relevance
CORRECT NO SLOWDOWN PREDICTIONS
NO SLOWDOWN COMPOSITE
(d)
(e)
0.0 0.1 0.2 0.3 0.4 0.5 0.6 0.7 0.8
LRP (Relevance)
-1.5 -1.0 -0.5 0.0 0.5 1.0 1.5
OHC100 (Normalized)

Figure 3.


(a)
ACTUAL SLOWDOWN
FUTURE DECADES
Slowdown
No Slowdown
PREDICTED SLOWDOWN
1990
1995
2000
2005
2010
2015
2020
(b)
Unfiltered IPO Index
2.5
2.0
1.5
1.0
0.5
0.0
-0.5
-1.0
-1.5
-2.0
-2.5
1990
1995
2000
2005
2010
2015
2020

Supporting Information for "Predicting slowdowns in decadal climate warming trends with explainable neural networks"

Zachary M. Labe[1]and Elizabeth A. Barnes[1]

[1]Department of Atmospheric Science, Colorado State University, Fort Collins, CO, USA

Contents of this file

0094-8276/22/$5.00

Text S1: Community Earth System Model Version 2 (CESM2)
CESM2 uses a nominal 1° horizontal resolution and includes 32 vertical levels with a model top at 2.26 hPa. Components for CESM2 include an atmosphere model from Community Atmosphere Model version 6 (CAM6; Danabasoglu et al., 2020) and an ocean model from Parallel Ocean Program Version 2 (POP2; Smith et al., 2010; Danabasoglu et al., 2012), which are further coupled to interactive ice, land, and ocean biogeochemistry models. Additional details on model development can be found in Danabasoglu et al. (2020). Overall, CESM2 scores well in comparison to other Coupled Model Intercomparison Project Phase 6 (CMIP6) models (e.g., Fasullo, 2020) and includes numerous improvements to cloud microphysics, the ocean surface boundary layer, and land processes over the previous model generation (CESM1; Hurrell et al., 2013; Kay et al., 2015). Future projections of global mean surface temperature (GMST) in CESM2 generally fall in the upper range of CMIP6 models, which is likely due to a higher equilibrium climate sensitivity (Gettelman et al., 2019; Meehl et al., 2020). Representation of the El Niño-Southern Oscillation (ENSO) and Pacific Decadal Oscillation (PDO) in CESM2 compare fairly well to observations, but there are still some large differences in simulated amplitude and spatial patterns (Capotondi et al., 2020; Chen et al., 2021).

Text S2: Artificial Neural Network Architecture
Artificial neural networks (ANNs) have become an increasingly popular method in the Earth sciences for their ability to capture nonlinear behavior in data-intensive problems and applications (Boukabara et al., 2021). In this work, we are not only interested in the skill of an ANN to predict warming slowdown events, but also the the opportunity to learn how the ANN is making correct predictions through a relatively new machine learning explainability method.

We provide an overview of the artificial neural network (ANN) used in our analysis in Figure S3. Our input layer receives vectorized maps of annual-mean ocean heat content in the 0-100 m depth (OHC100) from the CESM2 Large Ensemble Community Project (CESM2-LE), where each unit represents one grid box (13248 units per map from 92 latitudes by 144 longitudes). The input vector is then fed into two hidden layers with 30 nodes each, and our output layer contains two nodes (yes or no for a decadal warming slowdown). In this fully-connected neural network, each node receives a value from the previous layer. For example, each node of the first hidden layer is connected to every node in the second hidden layer. The value of a single node is calculated by weighting the sum of the inputs and an added bias term,

$$z_j = \sum_i w_{ij} x_i + b \tag{1}$$

where i is the node from the previous layer and j is the node for the value in the current layer (equation 1). In equation 1, w_{ij} denotes the weight between nodes i and j, x_i is the value of node i, and b is the added bias. The weights and biases are iteratively updated until the training is complete (i.e., minimized loss function). To include nonlinear transformations, we apply the rectified linear unit (ReLU; equation 2; Agarap, 2018) to our hidden nodes (z_j) and include a softmax operator in the output layer (equation 3). In equation 3, x_i represents the pre-softmax (raw) output for node i, and then $\tilde{y}_i$ is the final predicted output. The softmax function remaps the output values so that they sum to one and can then be interpreted as the ANN's confidence for each prediction output. For example, the winning predicted category (i.e., yes or no slowdown) will have a confidence value greater than 0.5.

$$f(z_j) = max(0, z_j) \tag{2}$$

$$\tilde{y}_i = \frac{\exp{(x_i)}}{\sum_{j=1} \exp{(x_j)}} \tag{3}$$

Our ANN uses a categorical cross-entropy loss function, where M is the number of classes, y_k is the true probability distribution, and $\hat{y}_k$ is the predicted probability distribution as denoted in equation 4. Due to the logarithmic transformation, this loss function penalizes larger errors more than smaller errors.

$$\text{Loss} = -\sum_{k=1}^{M} y_k \cdot \log{(\hat{y}_k)} \tag{4}$$

Before training our ANN, we standardize our maps of OHC100 by subtracting the mean and dividing by the standard deviation separately at every grid point and across all years for the training ensemble members (13248

units). Specifically, we train our ANN using 70% of the climate model data (28 ensemble members), validate on 15% (6 ensemble members), and test on the remaining 15% (6 ensemble members). We find that using at least 20 ensemble members for training corresponds to a better balance of recall and precision score metrics (Figure S2). Note that this is also larger than the minimum number of ensemble members needed for capturing global ENSO teleconnections as found in Lee et al. (2021).

During training, we use the stochastic gradient descent optimizer and turn on the Nesterov momentum parameter (set to 0.9) (Nesterov, 1983; Ruder, 2016). Our learning rate is set to 0.001, and the batch size is 128. Batch size refers to a subset of the training data, where the weights and biases are updated after each batch iteration. Thus, one epoch is completed after iterating through all of the training data. During this entire process, the ANN is attempting to minimize the loss function (i.e., reduce the error). While we set the ANN to train using 500 epochs, we apply early stopping on the validation loss to prevent overfitting. In the other words, the ANN is finished training if the validation loss does not improve for 10 epochs in a row. Using this approach, our ANN generally reaches no more than 35 epochs and is restored to the iteration with the best model weights.

To further account for overfitting, we apply L_2 ridge regularization (Friedman, 2012) to the weights of the first hidden layer. Our L_2 parameter is set to 0.5 after exploring several different combinations of ANN architectures, hyperparameters, and random initialization seeds (Figures S2-S3). Ridge regularization ensures the ANN is not sensitive to outlier weights, which helps to consider any spatial autocorrelation in the input fields of OHC100. Finally, we assign class weights in the loss function, since there is a large class imbalance with only 16 or fewer slowdown events per individual ensemble member (Figure 1c). This parameters tells the model to pay more attention to the underrepresented class during the training process. Figure S6 shows the results of ANNs using a range of class weights compared to the original class imbalance (approximately 8.8 to 1). For the main figures and analysis presented here, we selected a smaller fraction to be applied to the balanced class weights (approximately 4.4 to 1).

Given the large class imbalance (i.e., fewer number of slowdown training samples compared to non-slowdowns), we evaluate the results of our ANN using the F1 score (Johnson & Khoshgoftaar, 2019). The F1 score is a harmonic mean of the ANN's precision and recall (equation 5). Here, precision is a measure of how many predicted slowdowns are actually slowdown events (equation 6), and recall is a measure of how many actual slowdowns are correctly predicted as slowdowns (equation 7). We find an ANN architecture of this complexity achieves a reasonable F1 score (Figures S2-S3), which is higher than random chance (Section 3.1). Note that we present the results of our ANN used in the main analysis of the paper in Figure S7 using a confusion matrix for a binary classification problem (Shultz & Fahlman, 2017).

$$\mathrm{F1} = 2 \times \frac{\mathrm{Precision} * \mathrm{Recall}}{\mathrm{Precision} + \mathrm{Recall}} \tag{5}$$

$$\mathrm{Precision} = \frac{\mathrm{True\ Positive}}{\mathrm{True\ Positive} + \mathrm{False\ Positive}} \tag{6}$$

$$\mathrm{Recall} = \frac{\mathrm{True\ Positive}}{\mathrm{True\ Positive} + \mathrm{False\ Negative}} \tag{7}$$

In summary, this general approach and set of score metrics are commonly used for many neural network classification problems (Goodfellow et al., 2016). More resources on neural networks can be found in e.g., Lecun, Bengio, and Hinton (2015); Goodfellow et al. (2016); Neapolitan and Jiang (2018); A.Géron (2019).

Text S3: Open Software/Tools

Preprocessing and regridding were completed using NCL v6.2.2 (NCAR, 2019), NCO v4.9.3 (Zender, 2008), and CDO v1.9.8 (Schulzweida, 2019). Figures and main analysis were completed using open source Python v3.7.6, Numpy v1.19 (Harris et al., 2020), SciPy v1.4.1 (Virtanen et al., 2020), Matplotlib v3.2.2 (Hunter, 2007), and colormaps provided by cmocean v2.0 (Thyng et al., 2016), Palettable's cubehelix v3.3.0 (Green, 2011), and Scientific v7.0.0 (Crameri, 2018; Crameri et al., 2020). Additional Python packages used for development of the ANN and LRP visualizations include TensorFlow v2.4.0/v1.15.0 (Abadi et al., 2016), Scikit-learn v0.24.2 (Pedregosa et al., 2011), and iNNvestigate v1.0.8 (Alber et al., 2019). References for the data sets are provided throughout the study. Lastly, we would like to thank all the scientists, software engineers, and administrators who contributed to the development of CESM2.

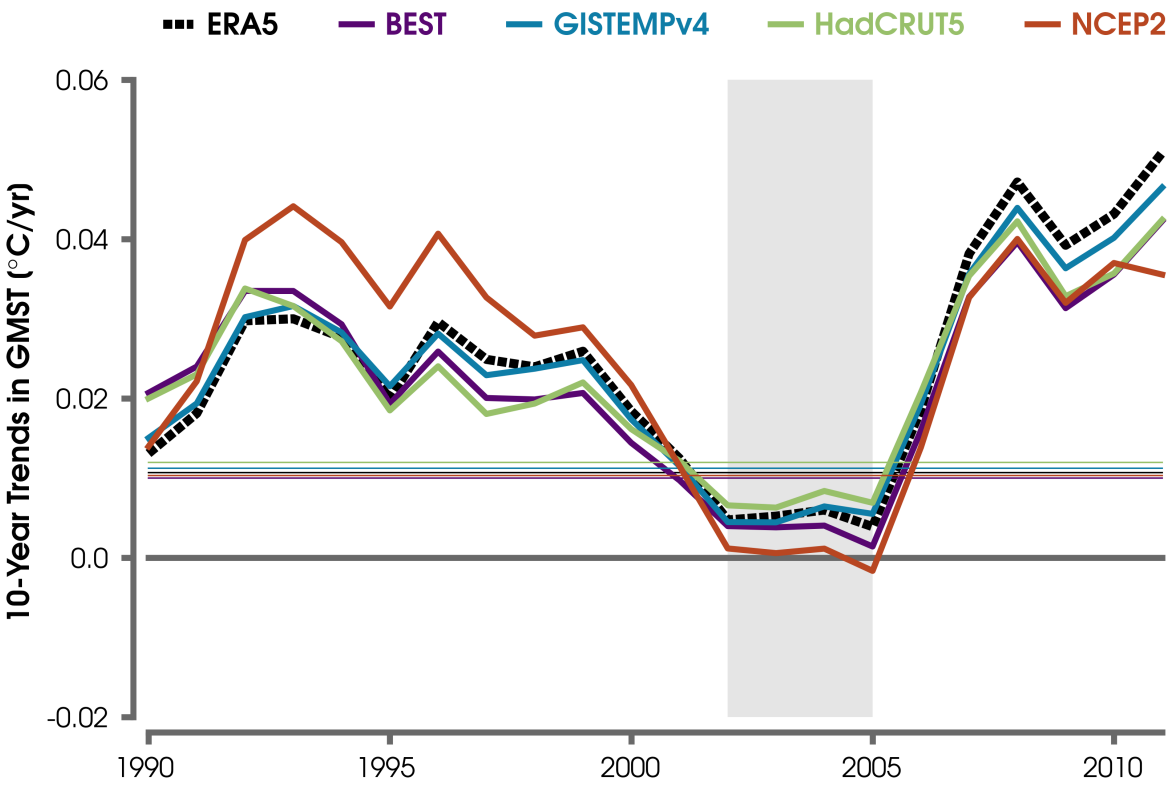

Figure S1. The slope of linear trends are calculated for each decade of global mean (near-) surface temperatures from 1990 to 1999 and ending in 2011 to 2020 using European Centre for Medium-Range Weather Forecasts ERA5 (dashed black line) reanalysis (Hersbach et al., 2020), Berkeley Earth Land/Ocean Temperature Record (BEST; solid purple line) (Rohde & Hausfather, 2020), Goddard Institute for Space Studies Surface Temperature product version 4 (GISTEMPv4; solid blue line) (Hansen et al., 2010; Lenssen et al., 2019), Hadley Centre/Climatic Research Unit Temperature version 5.0.1.0 (HadCRUT5; solid green line) dataset (Morice et al., 2021), and National Centers for Environmental Prediction–Department of Energy Reanalysis II (NCEP2; solid orange line) (Kanamitsu et al., 2002). Gray shading shows the onset of actual slowdown events in ERA5 reanalysis (as in Figure 3's green bars). Horizontal solid lines indicate the threshold for slowdown events in each observational data set respectively. The thicker horizontal gray line denotes a trend of 0°C/yr.

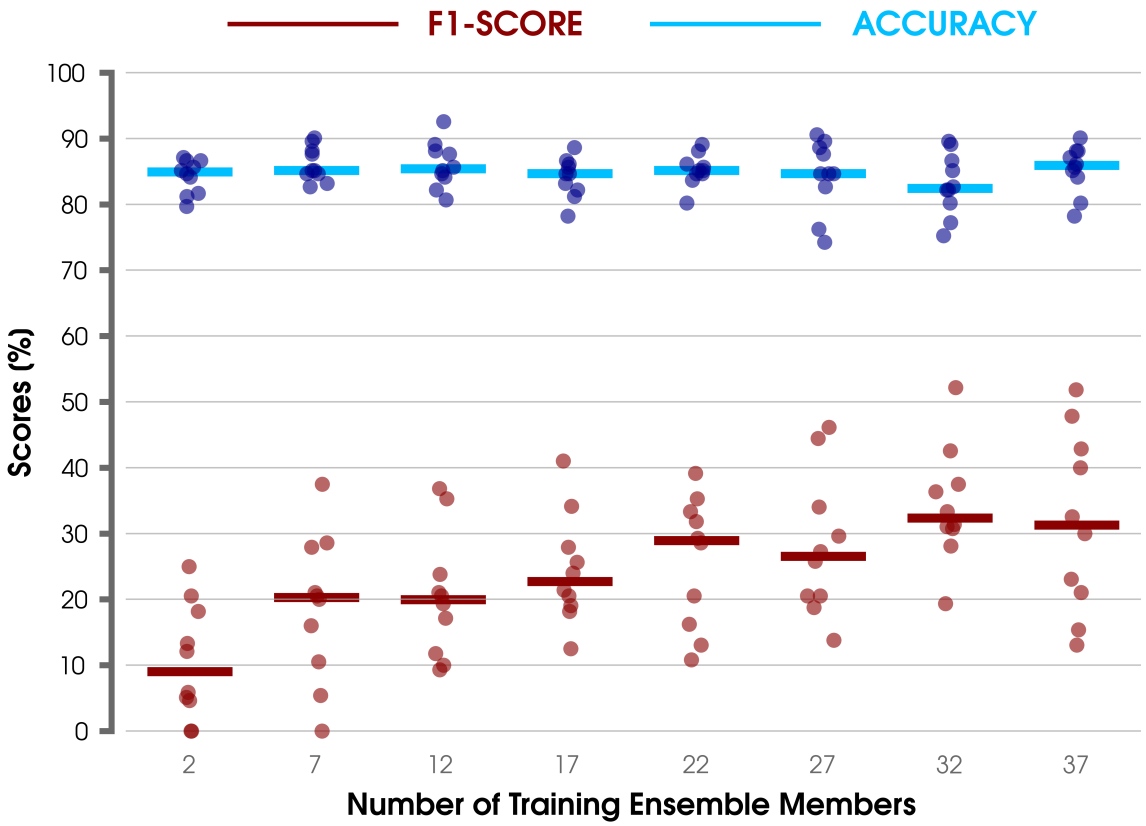

Figure S2. Points showing the accuracy (blue) and F1 score (red) for testing data. Results are shown for ANNs using a different number of training ensemble members from CESM2-LE (2, 7, 12, 17, 22, 27, 32, and 37 ensembles), but the same architecture as used in the paper (see Text S2 and Figure S3). For these different ANNs, 2 ensemble members are always used for testing data, and 1 ensemble member is always used for validation data. The points for each ANN experiment are comprised of 10 iterations (different combinations of training, testing, and validation data and random initialization seeds), and the median score is shown for each set of points with a bold horizontal line respectively. Note that the ANN used in the main analysis uses 28 ensembles for training data.

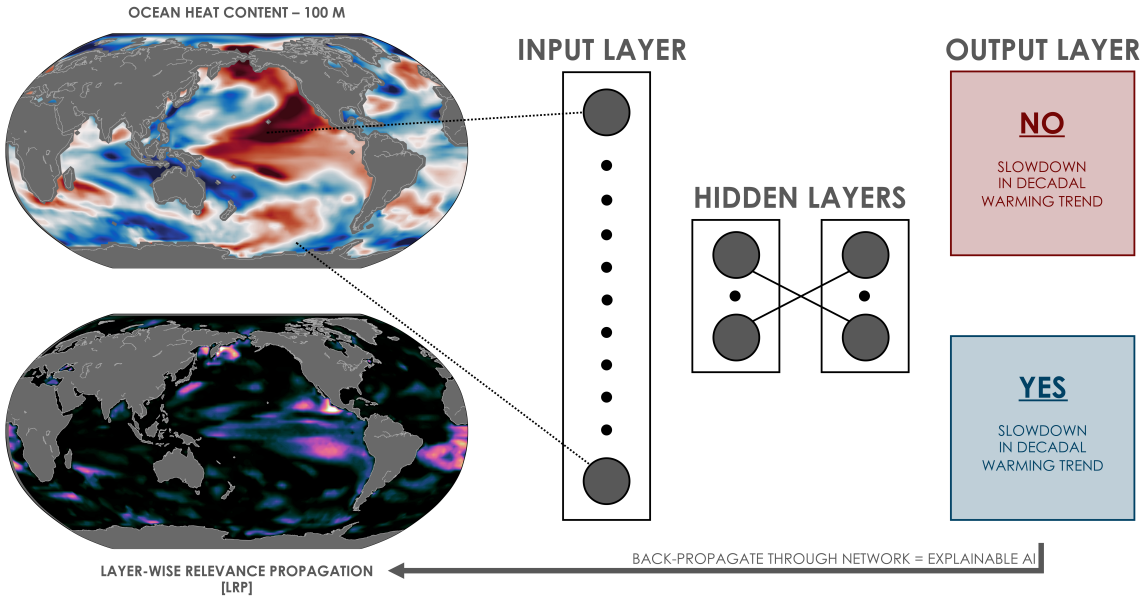

Figure S3. Schematic of the artificial neural network (ANN) used in this study for predicting the onset of a slowdown in decadal warming trend (output layer) from a global map of annual mean ocean heat content in the 0-100 m depth (input layer). The ANN consists of two hidden layers that both contain 30 hidden nodes. The output layer includes a softmax activation function. An example heatmap using layer-wise relevance propagation (LRP; Bach et al., 2015; Montavon et al., 2018) is also illustrated here. LRP highlights the regions of greater relevance for the ANN to decide whether a slowdown event will occur for the next 10 years.

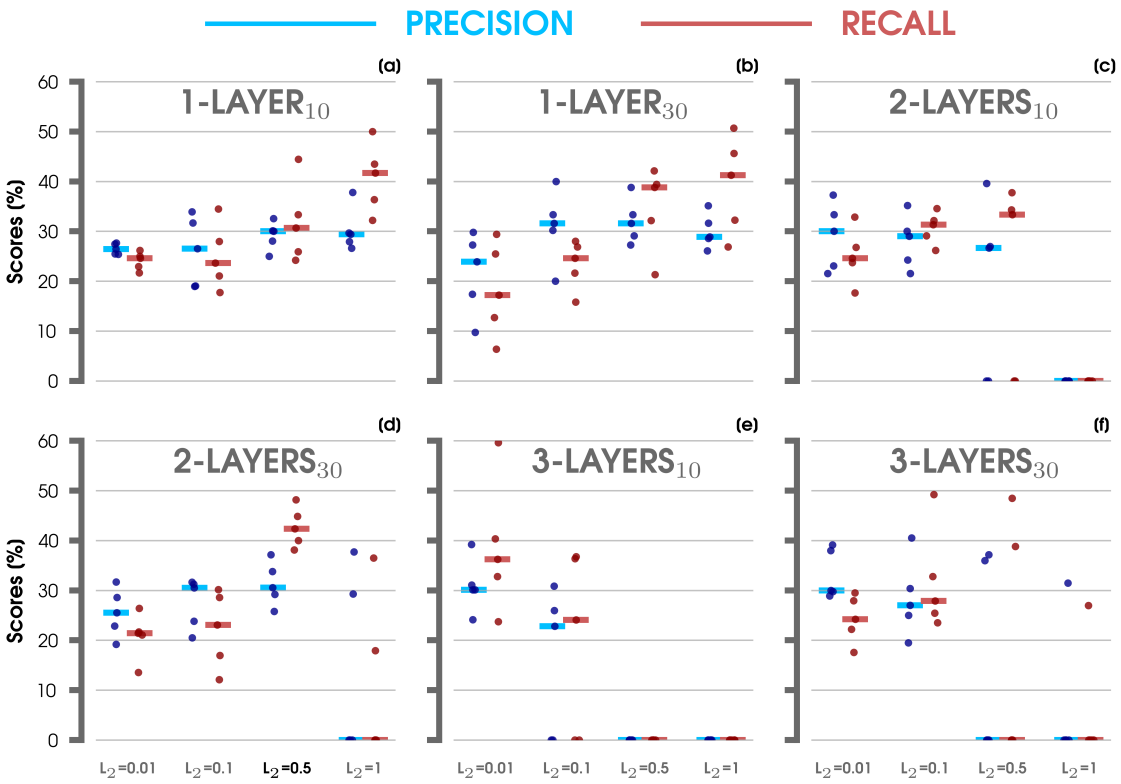

Figure S4. Points showing the precision (blue) and recall (red) scores for validation data. Results are shown for ANN architectures using (a) 1 hidden layers of 10 nodes, (b) 1 hidden layers of 30 nodes, (c) 2 hidden layers of 10 nodes each, (d) 2 hidden layers of 30 nodes each, (e) 3 hidden layers of 10 nodes each, (f) and 3 hidden layers of 30 nodes each (f). Each architecture also compares scores for different L_2 regularization values (0.01, 0.1, 0.5, 1). The points for each ANN are comprised of 5 iterations (different combinations of training, testing, and validation data and random initialization seeds), and the median score is shown for each set of points with a bold horizontal line respectively. The architecture used in the main analysis is labeled in bold for 2 hidden layers of 30 nodes each (subplot d).

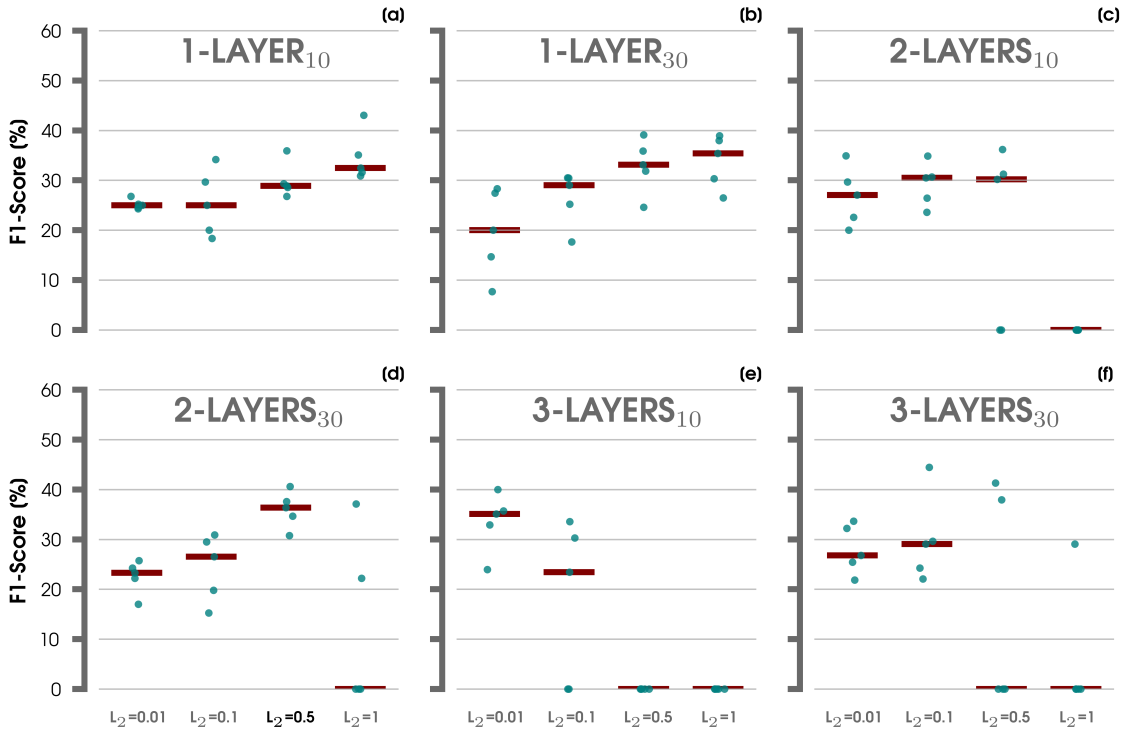

Figure S5. Points showing the F1 score for validation data. Results are shown for ANN architectures using (a) 1 hidden layers of 10 nodes, (b) 1 hidden layers of 30 nodes, (c) 2 hidden layers of 10 nodes each, (d) 2 hidden layers of 30 nodes each, (e) 3 hidden layers of 10 nodes each, (f) and 3 hidden layers of 30 nodes each (f). Each architecture also compares scores for different L_2 regularization values (0.01, 0.1, 0.5, 1). The points for each ANN are comprised of 5 iterations (different combinations of training, testing, and validation data and random initialization seeds), and the median score is shown for each set of points with a bold horizontal line respectively. The architecture used in the main analysis is labeled in bold for 2 hidden layers of 30 nodes each (subplot d).

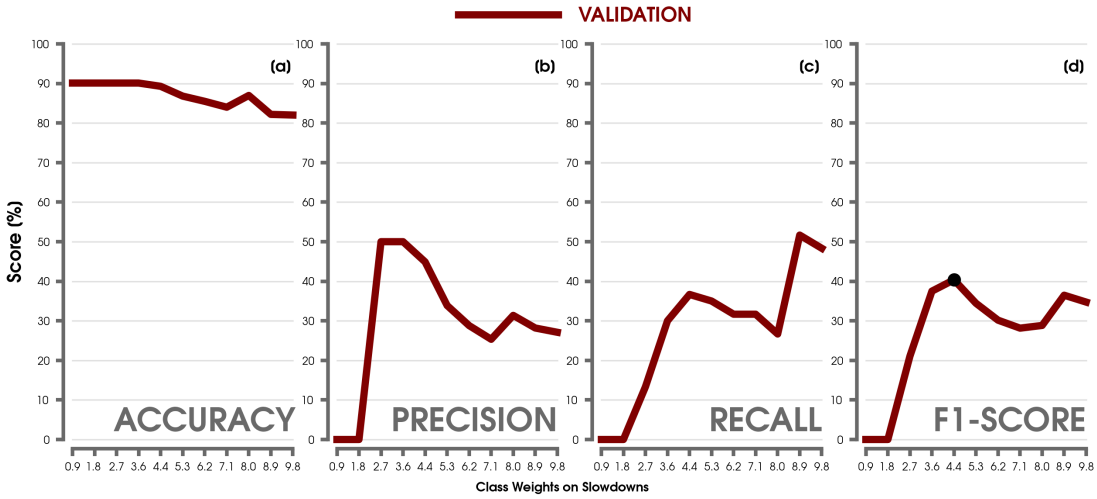

Figure S6. (a) Accuracy, (b) precision, (c) recall, (d) and F1 scores for validation data in the ANN architecture used throughout the paper, but with different class weights on slowdown events. The class weight used in the main analysis is shown with a marker for the F1 score.

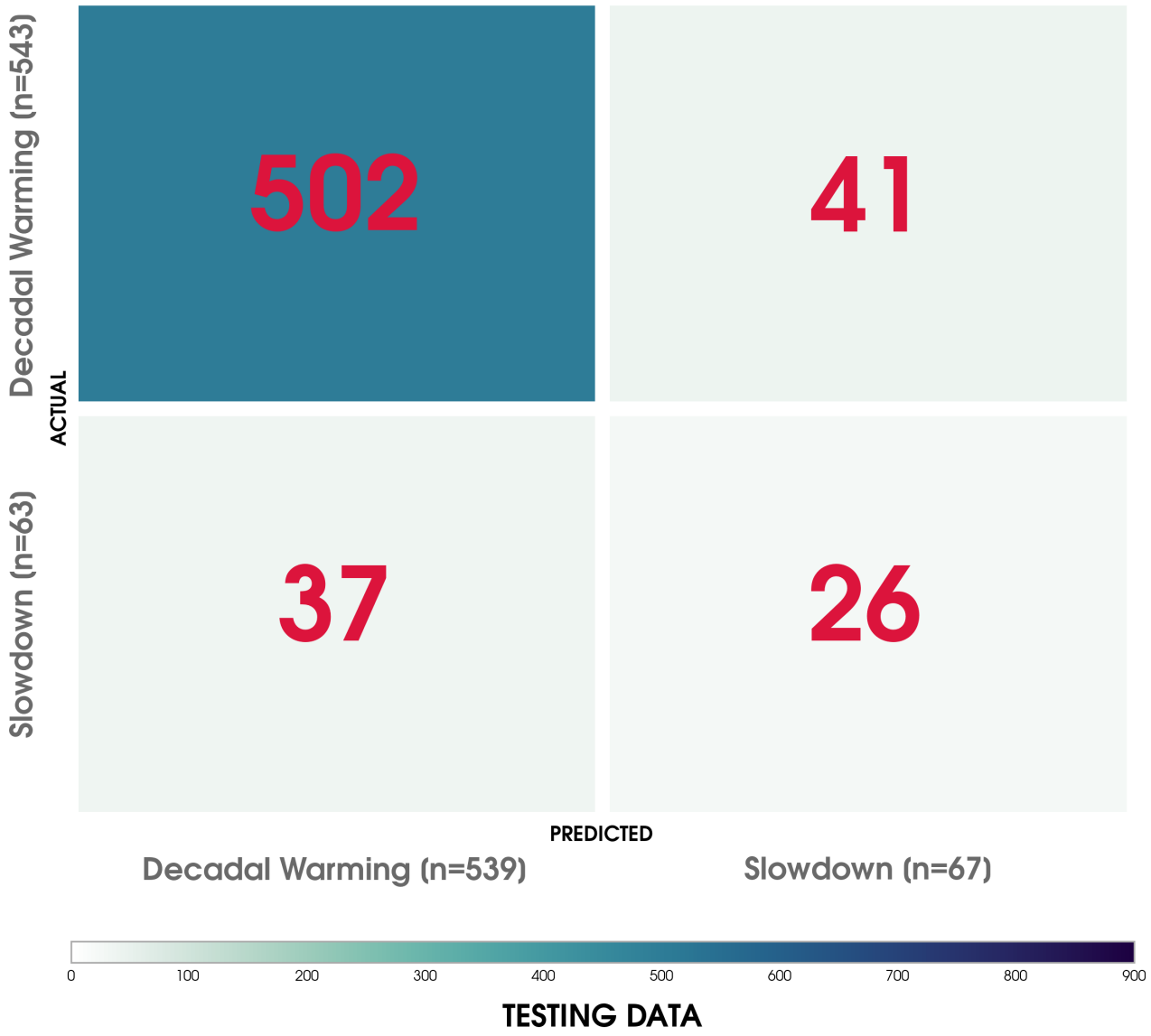

Figure S7. Confusion matrix of testing data for all predictions. The shading and large red values inside each box represents the sample size (n) for each classification category bin.

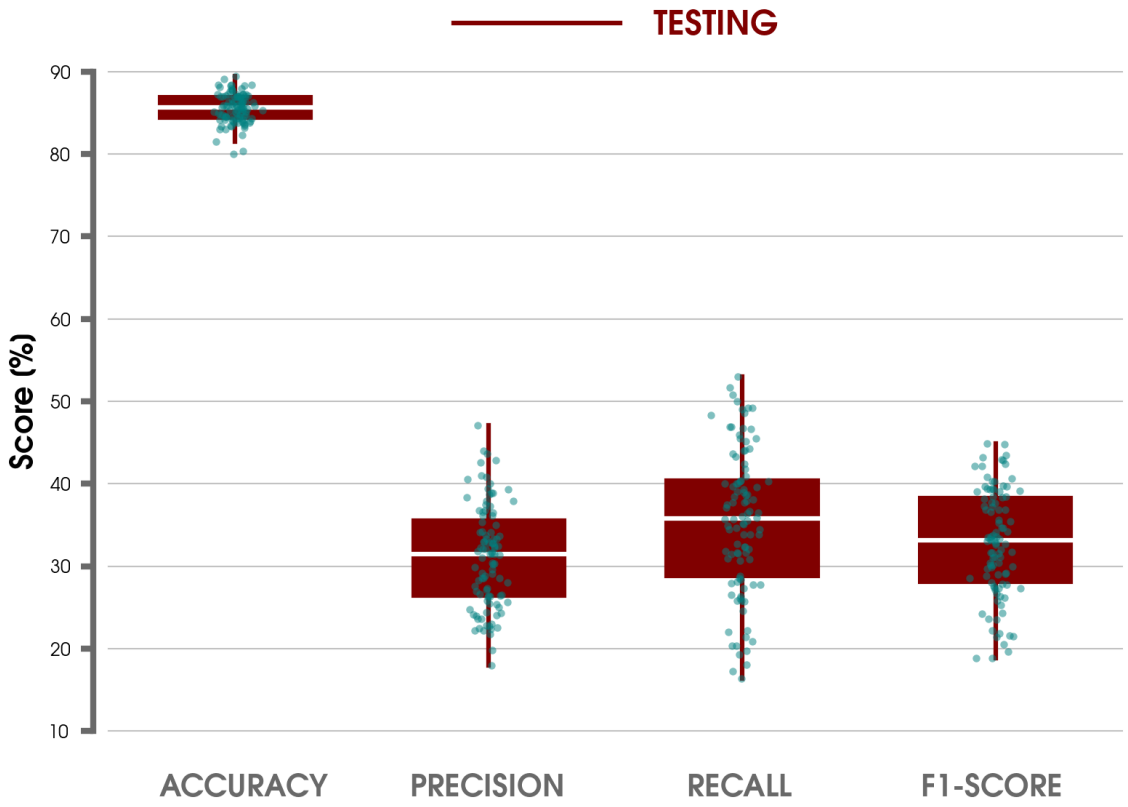

Figure S8. Box-and-whisker plots showing the accuracy, precision, recall, and F1 scores for the ANN architecture used throughout the paper after considering 100 different combinations of training, testing, and validation data and random initialization seeds.

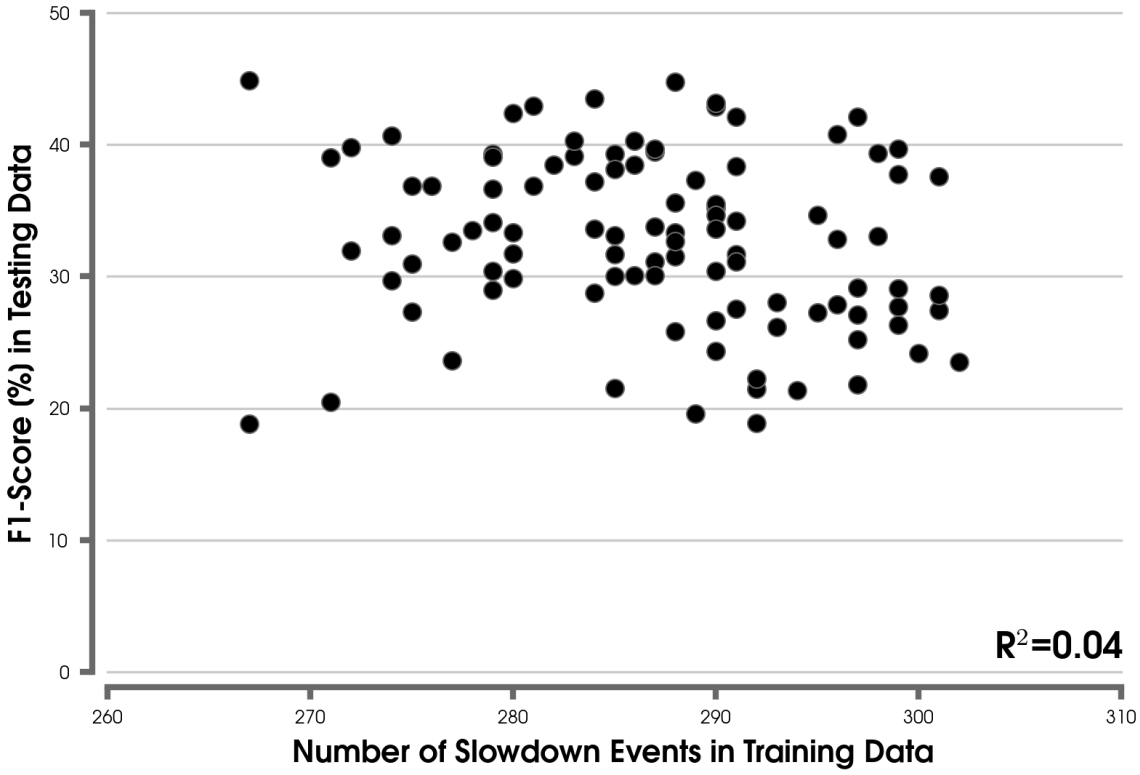

Figure S9. Scatter plot showing the number of slowdown events in training data compared to the F1 score for testing data in 100 ANNs using different combinations of training, testing, and validation data and random initialization seeds.

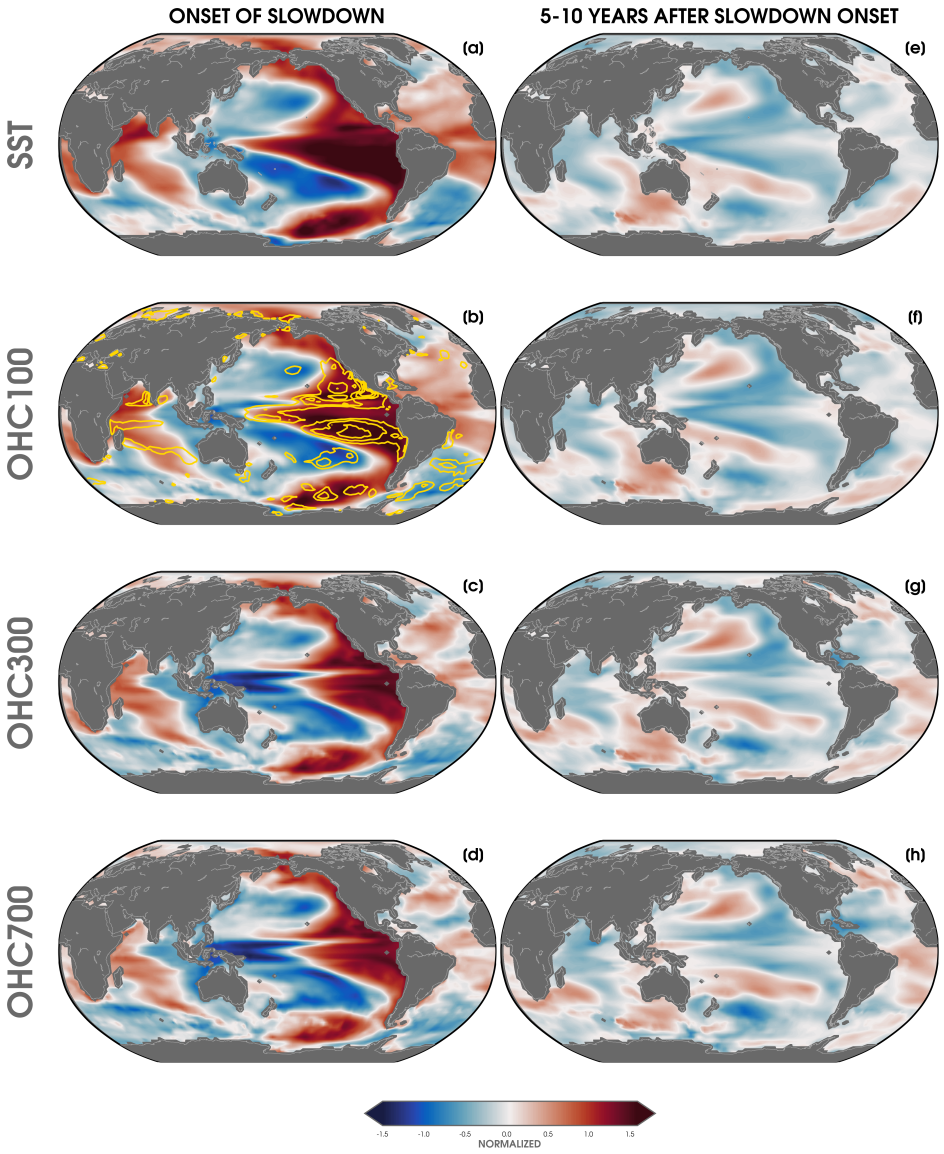

Figure S10. (a) Composite of normalized sea surface temperature (SST) for correct slowdown predictions by the ANN. (b) As in (a), but for ocean heat content in the 0-100 m layer (OHC100). Yellow contour lines are overlaid to show relevance from the LRP composite in main Figure 2b. (c) As in (a), but for ocean heat content in the 0-300 m layer (OHC300). (d) As in (a), but for ocean heat content in the 0-700 m layer (OHC700). (e-h) As in (a-d), but for composites of 5-10 years after the correct slowdown predictions.

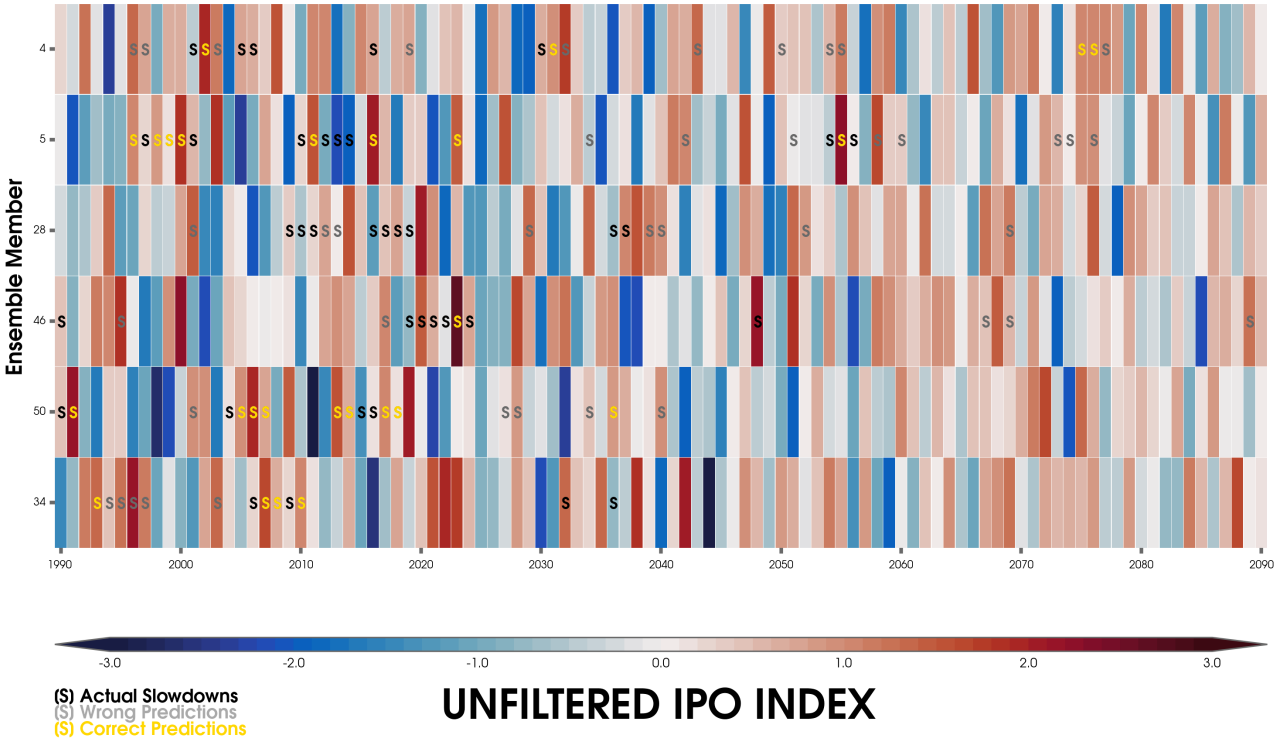

Figure S11. Unfiltered Tripole IPO Index (normalized) for each year of the six ensemble members in the testing data. Correct predictions by the ANN for the onset of slowdown events are highlighted with a yellow 'S' in each ensemble member, wrong slowdown predictions by the ANN are highlighted with a gray 'S' in each ensemble member, and all other actual slowdown events are indicated with a black 'S' in each ensemble member.

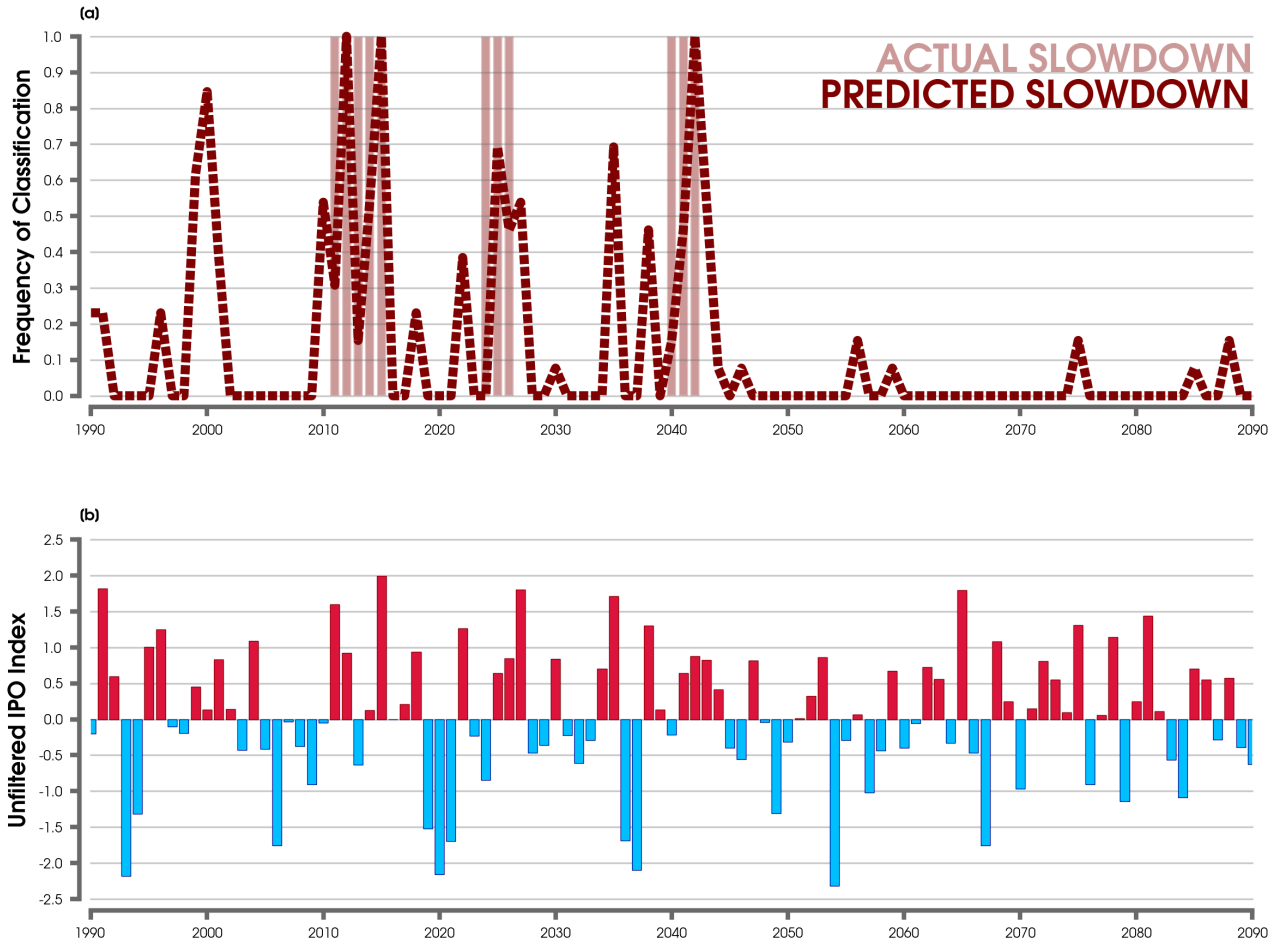

Figure S12. (a) Time series showing the frequency of slowdown onset predictions for one ensemble member realization (in testing data) using 13 ANNs constructed from different combinations of training, testing, and validation data (dashed dark red line). Light red bars show the onset of actual slowdown events in the ensemble member. (b) Time series of the unfiltered Tripole IPO Index (normalized) for each year in the same ensemble member (red/blue bars).

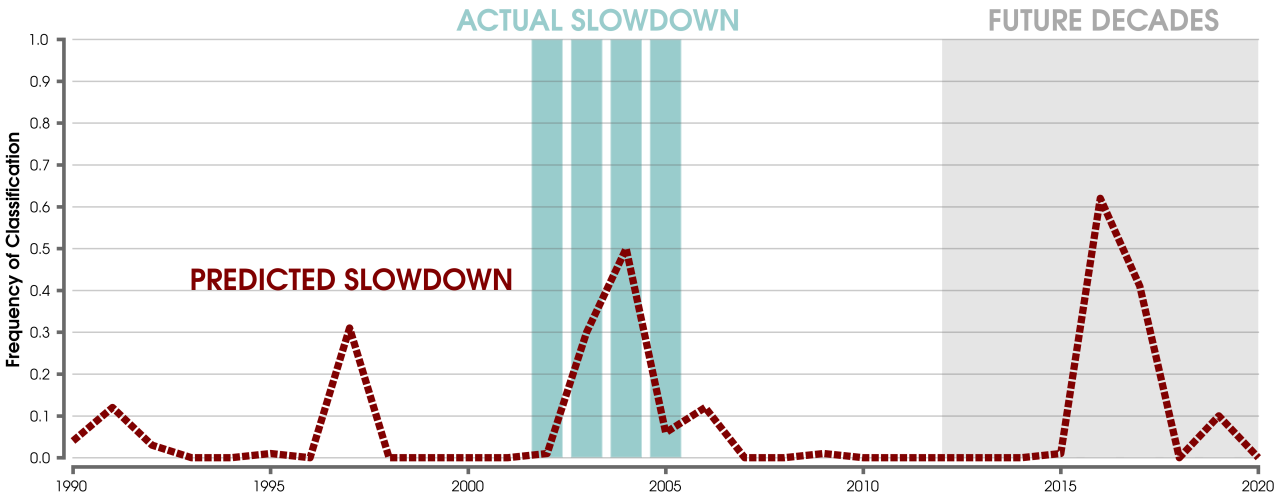

Figure S13. Time series showing the frequency of slowdown onset predictions after inputting observations into 100 ANNs constructed from different combinations of training, testing, and validation data. Green bars show the onset of actual slowdown events in observations. Gray shading indicates 10-year trend periods that extend into the future (e.g., 2012-2021).

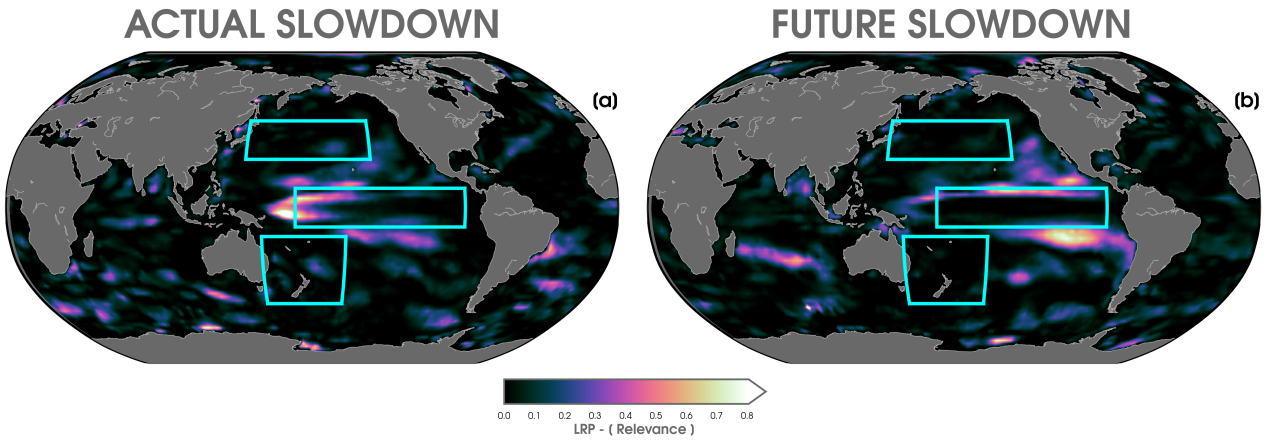

Figure S14. (a) LRP composite heatmap for the correct slowdown predictions by the ANN in observations. (b) As in (a), but for the ANN slowdown predictions during the future 10-year trend periods. Higher LRP values indicate greater relevance for the ANN's prediction. LRP values are normalized by the maximum relevance in the composite for visualization purposes. Blue boxes highlight regions of the Tripole Index for the IPO (Henley et al. (2015); 25°N-45°N and 140°E-145°W, 10°S-10°N and 170°E-90°W, 50°S-15°S and 150°E-160°W).

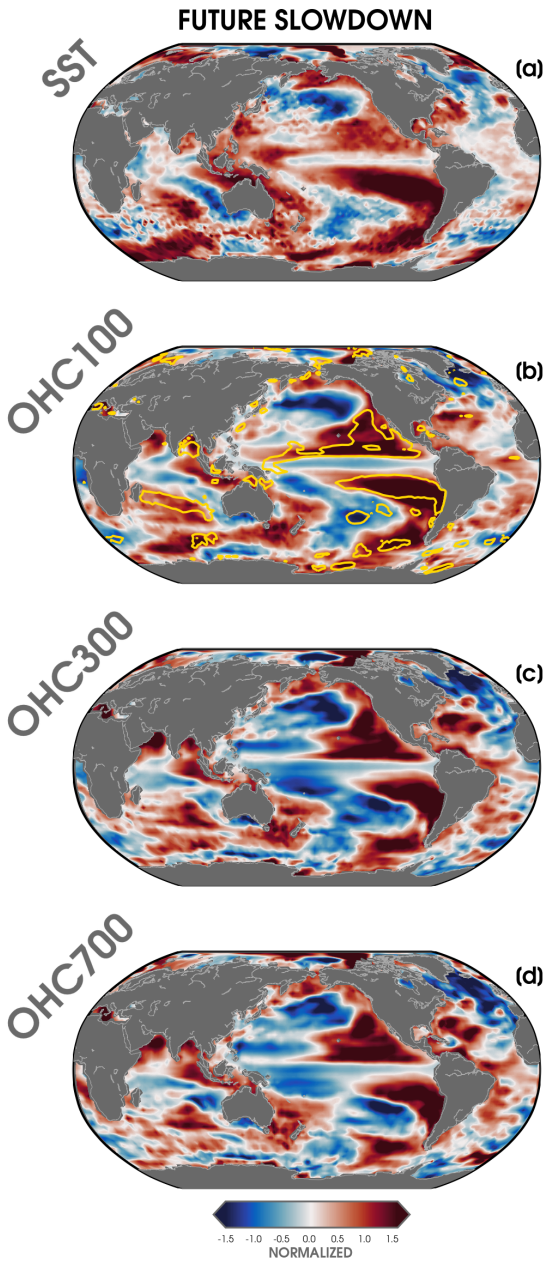

Figure S15. (a) Composite of normalized sea surface temperature (SST) for the future slowdown predictions after testing observations with the ANN. (b) As in (a), but for ocean heat content in the 0-100 m layer (OHC100). Yellow contour lines are overlaid to show relevance from the LRP composite in Figure S14b. (c) As in (a), but for ocean heat content in the 0-300 m layer (OHC300). (d) As in (a), but for ocean heat content in the 0-700 m layer (OHC700).

References

Abadi, M., Barham, P., Chen, J., Chen, Z., Davis, A., Dean, J., ... Zheng, X. (2016). TensorFlow: A system for large-scale machine learning. In *Proceedings of the 12th usenix symposium on operating systems design and implementation, osdi 2016.*

Agarap, A. F. (2018, mar). Deep Learning using Rectified Linear Units (ReLU). *arXiv*. Retrieved from http://arxiv.org/abs/1803.08375

A.Géron. (2019). *Hands-on machine learning with Scikit-Learn, Keras and TensorFlow: concepts, tools, and techniques to build intelligent systems.*

Alber, M., Lapuschkin, S., Seegerer, P., Hägele, M., Schütt, K. T., Montavon, G., ... Kindermans, P. J. (2019). INNvestigate neural networks! *Journal of Machine Learning Research*, *20*.

Bach, S., Binder, A., Montavon, G., Klauschen, F., Müller, K. R., & Samek, W. (2015, jul). On pixel-wise explanations for non-linear classifier decisions by layer-wise relevance propagation. *PLoS ONE*, *10*(7), e0130140. Retrieved from http://www.hfsp.org/, doi: 10.1371/journal.pone.0130140

Boukabara, S.-A., Krasnopolsky, V., Penny, S. G., Stewart, J. Q., McGovern, A., Hall, D., ... Hoffman, R. N. (2021, may). Outlook for Exploiting Artificial Intelligence in the Earth and Environmental Sciences. *Bulletin of the American Meteorological Society*, *102*(5), E1016–E1032. Retrieved from https://journals.ametsoc.org/view/journals/bams/102/5/BAMS-D-20-0031.1.xml doi: 10.1175/BAMS-D-20-0031.1

Capotondi, A., Deser, C., Phillips, A. S., Okumura, Y., & Larson, S. M. (2020, dec). ENSO and Pacific Decadal Variability in the Community Earth System Model Version 2. *Journal of Advances in Modeling Earth Systems*, *12*(12), e2019MS002022. Retrieved from https://agupubs.onlinelibrary.wiley.com/doi/10.1029/2019MS002022 doi: 10.1029/2019MS002022

Chen, H.-C., Fei-Fei-Jin, Zhao, S., Wittenberg, A. T., & Xie, S. (2021, dec). ENSO Dynamics in the E3SM-1-0, CESM2, and GFDL-CM4 Climate Models. *Journal of Climate*, *34*(23), 9365–9384. Retrieved from https://journals.ametsoc.org/view/journals/clim/34/23/JCLI-D-21-0355.1.xml doi: 10.1175/JCLI-D-21-0355.1

Crameri, F. (2018, jan). Scientific colour maps. *Zenodo*. Retrieved from https://zenodo.org/record/4153113 doi: 10.5281/ZENODO.4153113

Crameri, F., Shephard, G. E., & Heron, P. J. (2020, dec). The misuse of colour in science communication. *Nature Communications*, *11*(1), 1–10. Retrieved from https://doi.org/10.1038/s41467-020-19160-7 doi: 10.1038/s41467-020-19160-7

Danabasoglu, G., Bates, S. C., Briegleb, B. P., Jayne, S. R., Jochum, M., Large, W. G., ... Yeager, S. G. (2012). The CCSM4 ocean component. *Journal of Climate*, *25*(5). doi: 10.1175/JCLI-D-11-00091.1

Danabasoglu, G., Lamarque, J.-F., Bacmeister, J., Bailey, D. A., DuVivier, A. K., Edwards, J., ... Strand, W. G. (2020, feb). The Community Earth System Model Version 2 (CESM2). *Journal of Advances in Modeling Earth Systems*, *12*(2), e2019MS001916. Retrieved from https://agupubs.onlinelibrary.wiley.com/doi/10.1029/2019MS001916 doi: 10.1029/2019MS001916

Fasullo, J. T. (2020, aug). Evaluating simulated climate patterns from the CMIP archives using satellite and reanalysis datasets using the Climate Model Assessment Tool (CMATv1). *Geoscientific Model Development*, *13*(8), 3627–3642. doi: 10.5194/GMD-13-3627-2020

Friedman, J. H. (2012, jul). Fast sparse regression and classification. *International Journal of Forecasting*, *28*(3), 722–738. doi: 10.1016/j.ijforecast.2012.05.001

Gettelman, A., Hannay, C., Bacmeister, J. T., Neale, R. B., Pendergrass, A. G., Danabasoglu, G., ... Mills, M. J. (2019, jul). High Climate Sensitivity in the Community Earth System Model Version 2 (CESM2). *Geophysical Research Letters*, *46*(14), 8329–8337. Retrieved from https://agupubs.onlinelibrary.wiley.com/doi/10.1029/2019GL083978 doi: 10.1029/2019GL083978

Goodfellow, I., Bengio, Y., & Courville, A. (2016). *Deep Learning.*

Green, D. A. (2011). A colour scheme for the display of astronomical intensity images. *Bulletin of the Astronomical Society of India*, *39*(2).

Hansen, J., Ruedy, R., Sato, M., & Lo, K. (2010, dec). GLOBAL SURFACE TEMPERATURE CHANGE. *Reviews of Geophysics*, *48*(4), 4004. Retrieved from https://agupubs.onlinelibrary.wiley.com/doi/10.1029/2010RG000345 doi: 10.1029/2010RG000345

Harris, C. R., Jarrod Millman, K., van der Walt, S. J., Gommers, R., Virtanen, P., Cournapeau, D., ... Oliphant, T. E. (2020, sep). Array programming with NumPy. *Nature*, *585*(7825), 357. Retrieved from https://doi.org/10.1038/s41586-020-2649-2 doi: 10.1038/s41586-020-2649-2

Henley, B. J., Gergis, J., Karoly, D. J., Power, S., Kennedy, J., & Folland, C. K. (2015). A Tripole Index for the Interdecadal Pacific Oscillation. *Climate Dynamics*. doi: 10.1007/s00382-015-2525-1

Hersbach, H., Bell, B., Berrisford, P., Hirahara, S., Horányi, A., Muñoz-Sabater, J., ... Thépaut, J.-N. (2020, may). The ERA5 Global Reanalysis. *Quarterly Journal of the Royal Meteorological Society*. Retrieved from https://onlinelibrary.wiley.com/doi/abs/10.1002/qj.3803 doi: 10.1002/qj.3803

Hunter, J. D. (2007, may). Matplotlib: A 2D graphics environment. *Computing in Science and Engineering*, *9*(3), 99–104. doi: 10.1109/MCSE.2007.55

Hurrell, J. W., Holland, M. M., Gent, P. R., Ghan, S., Kay, J. E., Kushner, P. J., ... Marshall, S. (2013). The community earth system model: A framework for collaborative research. *Bulletin of the American Meteorological Society*, *94*(9). doi: 10.1175/BAMS-D-12-00121.1

Johnson, J. M., & Khoshgoftaar, T. M. (2019). Survey on deep learning with class imbalance. *Journal of Big Data*, *6*(1). doi: 10.1186/s40537-019-0192-5

Kanamitsu, M., Ebisuzaki, W., Woollen, J., Yang, S.-K., Hnilo, J. J., Fiorino, M., & Potter, G. L. (2002, nov). NCEP–DOE AMIP-II Reanalysis (R-2). *Bulletin of the American Meteorological Society*, *83*(11), 1631–1643. Retrieved from http://journals.ametsoc.org/doi/abs/10.1175/BAMS-83-11-1631 doi: 10.1175/BAMS-83-11-1631

Kay, J. E., Deser, C., Phillips, A., Mai, A., Hannay, C., Strand, G., ... Vertenstein, M. (2015, aug). The Community Earth System Model (CESM) Large Ensemble Project: A Community Resource for Studying Climate Change in the Presence of Internal Climate Variability. *Bulletin of the American Meteorological Society*, *96*(8), 1333–1349. Retrieved from http://journals.ametsoc.org/doi/10.1175/BAMS-D-13-00255.1 doi: 10.1175/BAMS-D-13-00255.1

Lecun, Y., Bengio, Y., & Hinton, G. (2015, may). *Deep learning* (Vol. 521) (No. 7553). Nature Publishing Group. Retrieved from https://www.nature.com/articles/nature14539 doi: 10.1038/nature14539

Lee, J., Planton, Y. Y., Gleckler, P. J., Sperber, K. R., Guilyardi, E., Wittenberg, A. T., ... Pallotta, G. (2021, oct). Robust Evaluation of ENSO in Climate Models: How Many Ensemble Members Are Needed? *Geophysical Research Letters*, *48*(20), e2021GL095041. Retrieved from https://agupubs-onlinelibrary-wiley-com.ezproxy2.library.colostate.edu doi: 10.1029/2021GL095041

Lenssen, N. J. L., Schmidt, G. A., Hansen, J. E., Menne, M. J., Persin, A., Ruedy, R., & Zyss, D. (2019, jun). Improvements in the GISTEMP Uncertainty Model. *Journal of Geophysical Research: Atmospheres*, *124*(12), 6307–6326. Retrieved from https://onlinelibrary.wiley.com/doi/abs/10.1029/2018JD029522 doi: 10.1029/2018JD029522

Meehl, G. A., Arblaster, J. M., Bates, S., Richter, J. H., Tebaldi, C., Gettelman, A., ... Strand, G. (2020, sep). Characteristics of Future Warmer Base States in CESM2. *Earth and Space Science*, *7*(9), e2020EA001296. Retrieved from https://agupubs.onlinelibrary.wiley.com/doi/10.1029/2020EA001296 doi: 10.1029/2020EA001296

Montavon, G., Samek, W., & Müller, K. R. (2018, feb). *Methods for interpreting and understanding deep neural networks* (Vol. 73). Elsevier Inc. doi: 10.1016/j.dsp.2017.10.011

Morice, C. P., Kennedy, J. J., Rayner, N. A., Winn, J. P., Hogan, E., Killick, R. E., ... Simpson, I. R. (2021, feb). An Updated Assessment of Near-Surface Temperature Change From 1850: The HadCRUT5 Data Set. *Journal of Geophysical Research: Atmospheres*, *126*(3), e2019JD032361. Retrieved from https://agupubs.onlinelibrary.wiley.com/doi/10.1029/2019JD032361 doi: 10.1029/2019JD032361

NCAR. (2019). *The NCAR Command Language (Version 6.6.2)*. Boulder, Colorado. Retrieved from http://dx.doi.org/10.5065/D6WD3XH5 doi: http://dx.doi.org/10.5065/D6WD3XH5

Neapolitan, R. E., & Jiang, X. (2018, nov). Neural Networks and Deep Learning. In *Artificial intelligence* (pp. 389–411). Chapman and Hall/CRC. doi: 10.1201/b22400-15

Nesterov, Y. (1983). A method for unconstrained convex minimization problem with the rate of convergence o(1/kˆ2). *Doklady AN USSR*, *269*.

Pedregosa, F., Varoquaux, G., Gramfort, A., Michel, V., Thirion, B., Grisel, O., ... Duchesnay, É. (2011). Scikit-learn: Machine learning in Python. *Journal of Machine Learning Research*, *12*.

Rohde, R. A., & Hausfather, Z. (2020, dec). The Berkeley Earth Land/Ocean Temperature Record. *Earth System Science Data*, *12*(4), 3469–3479. Retrieved from https://essd.copernicus.org/articles/12/3469/2020/ doi: 10.5194/essd-12-3469-2020

Ruder, S. (2016, sep). An overview of gradient descent optimization algorithms. *arXiv*. Retrieved from http://arxiv.org/abs/1609.04747

Schulzweida, U. (2019, feb). CDO User Guide. *Zenodo*. Retrieved from https://zenodo.org/record/2558193 doi: 10.5281/ZENODO.2558193

Shultz, T. R., & Fahlman, S. E. (2017). Confusion Matrix. *Encyclopedia of Machine Learning and Data Mining*, 260–260. Retrieved from https://link.springer.com/referenceworkentry/10.1007/978-1-4899-7687

-1{_}50 doi: 10.1007/978-1-4899-7687-1_50

Smith, R., Jones, P., Briegleb, B., Bryan, F., Danabasoglu, G., Dennis, J., ... Yeager, S. (2010). The Parallel Ocean Program (POP) reference manual: Ocean component of the Community Climate System Model (CCSM). *Rep. LAUR-01853*, *141*.

Thyng, K., Greene, C., Hetland, R., Zimmerle, H., & DiMarco, S. (2016, sep). True Colors of Oceanography: Guidelines for Effective and Accurate Colormap Selection. *Oceanography*, *29*(3), 9–13. Retrieved from https://tos.org/oceanography/article/true-colors-of-oceanography-guidelines-for-effective-and-accurate-colormap doi: 10.5670/oceanog.2016.66

Virtanen, P., Gommers, R., Oliphant, T. E., Haberland, M., Reddy, T., Cournapeau, D., ... Vázquez-Baeza, Y. (2020). SciPy 1.0: fundamental algorithms for scientific computing in Python. *Nature Methods*, *17*(3). doi: 10.1038/s41592-019-0686-2

Zender, C. S. (2008). Analysis of self-describing gridded geoscience data with netCDF Operators (NCO). *Environmental Modelling and Software*, *23*(10-11). doi: 10.1016/j.envsoft.2008.03.004